JBC Papers in Press. Published on January 10, 2015 as Manuscript M114.610121
The latest version is at http://www.jbc.org/cgi/doi/10.1074/jbc.M114.610121

Aldo-Keto Reductase 1B15 (AKR1B15): a Mitochondrial Human Aldo-Keto Reductase with Activity towards Steroids and 3-Keto-acyl-CoA Conjugates*

Susanne Weber[1], Joshua K. Salabei[2], Gabriele Möller[1], Elisabeth Kremmer[3], Aruni Bhatnagar[2], Jerzy Adamski[1,4,5, §], and Oleg A. Barski[2, §]

[1] Helmholtz Zentrum Muenchen, German Research Center for Environmental Health, Institute of Experimental Genetics, Genome Analysis Center, 85764 Neuherberg, Germany
[2] Diabetes and Obesity Center, School of Medicine, University of Louisville, Louisville, KY 40202, USA
[3] Helmholtz Zentrum Muenchen, German Research Center for Environmental Health, Institute of Molecular Immunology, 81377 Muenchen, Germany
[4] Lehrstuhl für Experimentelle Genetik, Technische Universitaet Muenchen, 85356 Freising-Weihenstephan, Germany
[5] German Center for Diabetes Research, 85764 Neuherberg, Germany

*Running title: *Characterization of human AKR1B15*

§ To whom correspondence should be addressed:
Oleg A. Barski, NIGMS, NIH, 45 Center Dr. Rm. 2AS55C, Bethesda, MD 20892, USA. Tel: (301)-496-1511; Fax: (301)-480-2802; E-mail: oleg.barski@nih.gov (present address)[#]

or

Jerzy Adamski, Helmholtz Zentrum Muenchen, German Research Center for Environmental Health, Institute of Experimental Genetics, Genome Analysis Center, Ingolstaedter Landstr. 1, 85764 Neuherberg, Germany. Tel.: 049-89-3187-3155; Fax: 049-89-3187-3225; E-mail: Adamski@helmholtz-muenchen.de

[#]**Disclaimer:** This article was prepared while Oleg A. Barski was employed at the University of Louisville. The opinions expressed in this article are the author's own and do not reflect the view of the National Institutes of Health, the Department of Health and Human Services, or the United States government.

Keywords: Aldo-keto reductase (AKR), gene expression, enzyme kinetics, mitochondria, oxidation-reduction, 3-keto-acyl-CoA, steroids

Background: Aldo-keto reductases (AKRs) are enzymes involved in the metabolism of carbonyl substrates.
Results: Two alternatively-spliced protein isoforms encoded by the human AKR gene *AKR1B15* were identified. The AKR1B15.1 isoform catalyzes reduction of steroids and 3-keto-acyl-CoA conjugates and localizes to mitochondria.
Conclusion: AKR1B15.1 is a mitochondrial carbonyl reductase.
Significance: AKR1B15.1 is a new enzyme with unique localization and catalytic features.

ABSTRACT

Aldo-Keto Reductases (AKRs) comprise a superfamily of proteins involved in the reduction and oxidation of biogenic and xenobiotic carbonyls. In humans, at least 15 AKR superfamily members have been identified so far. One of these is a newly identified gene locus, *AKR1B15*, which clusters on chromosome 7 with the other human *AKR1B* subfamily members, i.e., *AKR1B1* and *AKR1B10*. We show that alternative splicing of the *AKR1B15* gene transcript gives rise to two protein isoforms with different N-termini: AKR1B15.1 is a 316 amino acid protein with 91 % amino acid identity to AKR1B10; AKR1B15.2 has a prolonged N-terminus and consists of 344 amino acid residues. The two gene products differ in their expression level, subcellular localization, and activity. In contrast with other AKR enzymes which are mostly cytosolic, AKR1B15.1 co-localizes with the mitochondria. Kinetic studies show that AKR1B15.1 is predominately a reductive enzyme that catalyzes the reduction of androgens and estrogens with high positional selectivity (17β-hydroxysteroid dehydrogenase activity) as well as 3-keto-acyl-CoAs and exhibits strong cofactor selectivity towards NADP(H). In accordance with its substrate spectrum, the enzyme is expressed at highest levels in steroid-sensitive tissues, namely placenta, testis, and adipose tissue. Placental and adipose expression could be reproduced in the BeWo and SGBS cell lines, respectively. In contrast, AKR1B15.2 localizes to the cytosol and displays no enzymatic activity with the substrates tested. Collectively, these results demonstrate the existence of a novel catalytically active AKR, which is associated with mitochondria and expressed mainly in steroid-sensitive tissues.

INTRODUCTION

The Aldo-Keto Reductase (AKR)[2] superfamily comprises 15 families containing over 150 members that are present in all phyla (1, 2). AKRs are multifunctional enzymes that catalyze the reduction of biogenic and xenobiotic aldehydes and ketones, as well as the synthesis and metabolism of sex hormones. The majority of AKRs catalyze oxidation-reduction reactions between carbonyl and alcohol groups, whereas enzymes of the AKR1D family reduce double bonds in the bile acid biosynthesis pathway acting as 5β-reductases (3). Some AKR proteins have very low or no activity and perform predominantly non-catalytic functions, e.g., structural (lens rho-crystallines: AKR1C10a and AKR1C10b) or regulatory and chaperone-like (voltage-gated potassium channel β-subunits of AKR6 family: Kvβ) functions (4, 5).
Prior to identification of AKR1B15, 14 human AKRs have been described. These proteins are generally cytosolic and monomeric with molecular weights ranging between 35-40 kDa. These enzymes catalyze oxidation-reduction reactions in a variety of cellular pathways such as glucose metabolism (AKR1B1) (2), vitamin C biosynthesis (AKR1A1) (6), steroid and prostaglandin metabolism (AKR1Bs and AKR1Cs) (7, 8), bile acid synthesis (AKR1D1) (9), neurotransmitter metabolism (AKR7) (10), as well as the detoxification of both endogenous oxidation by-products, such as advanced glycation end-product precursors or lipid peroxidation-derived aldehydes (11, 12), and exogenous toxins, such as aflatoxin B1 (13) or tobacco-derived carcinogen 4-methyl-nitrosamino-1-(3-pyridyl)-1-butanone (NNK) (14). Generally, the enzymes of the AKR superfamily prefer NADPH over NADH as a reducing cofactor (2, 15, 16).

The AKR1 family is the most numerous and has been further divided into 5 subfamilies (A-E). The AKR1B subfamily has been intensely studied due to the potential role of its founding member human aldose reductase (AKR1B1) in the development of diabetic complications (17, 18). Under hyper-glycemic conditions, AKR1B1 converts excess glucose into sorbitol, leading to osmotic and redox

imbalances and resulting in tissue injury associated with diabetes (19–21). Inhibition of AKR1B1 has been shown to prevent, delay or reverse tissue injury due to hyperglycemia (19, 22). In this context, a large number of studies and clinical trials have been devoted to find efficient inhibitors of aldose reductase to prevent the development of diabetic complications, however, these efforts have met limited success due to problems in trials design, low efficacy, and nonspecific side effects of inhibitors (17, 23). In addition to glucose, AKR1B1 catalyzes the reduction of several substrates of physiological significance including advanced glycation end-product precursors, 4-hydroxy-*trans*-2-nonenal, and oxidized phospholipids (11, 24, 25) and has been suggested to play important roles in the development of atherosclerosis (26), ischemic preconditioning (27), and restenosis (28).

AKR1B1 is closely related to the small intestine aldose reductase (AKR1B10) (29, 30). In contrast to *AKR1B1*, *AKR1B10* is expressed mainly in small intestine, colon, liver, thymus (29), and adrenal gland (30). AKR1B10 shares 71 % amino acid sequence identity with AKR1B1 and exhibits substrate specificity similar to aldose reductase with the exception that it has significantly higher catalytic efficiency with all-*trans*-retinal (31). *AKR1B10* is strongly overexpressed in lung and hepatic carcinomas (squamous cell and adeno-carcinomas) (29) as well as in colorectal and uterine cancers (32) and has been implicated in conferring resistance to anticancer drugs (33, 34).
Recently, a novel gene, *AKR1B15*, with 91 % identity to *AKR1B10* has been predicted in the genetic cluster encompassing *AKR1B1* and *AKR1B10* on human chromosome 7. We previously reported that this gene encodes a functional protein (35). However, in contrast to AKR1B1 and AKR1B10, the enzymatic activity of this newly identified AKR was low, and the protein expressed with N-terminal His-tag was found in the microsomal fraction in both the mammalian and bacterial expression systems (35). While orthologs of AKR1B1 are known in rodents (AKR1B3 in mouse and AKR1B4 in rat), direct orthology between AKR1B15 and AKR1B10 and rodent AKR1Bs has not been established so far.
In the present study we show that the *AKR1B15* gene gives rise to two alternatively spliced mRNA products, each coding for a unique protein, hereafter referred to as AKR1B15.1 and AKR1B15.2. Furthermore, we characterize the catalytic activity, tissue distribution, and subcellular localization of both AKR1B15 isoforms.

EXPERIMENTAL PROCEDURES

Chemicals and materials – Primers were synthesized by Integrated DNA Technology (IDT) or Metabion. Restriction enzymes and T4 DNA Ligase were obtained from either New England Biolabs (NEB) or Promega. Total RNA from human tissues was purchased from Clontech or ZenBio (adipose). Cofactors were purchased from Sigma (NAD^+; $NADP^+$; NADH) and Serva (NADPH). Unlabeled substrates were obtained from Sigma, whereas ^{3}H-labeled substrates were synthesized by American Radiolabeled Chemicals (cortisone [1,2-^{3}H(N)]), Amersham (17α-estradiol [6,9-^{3}H(N)]), and Perkin Elmer (3α,17β-androstanediol [9,11-^{3}H(N)]; androsterone [9,11-^{3}H(N)]; Δ4-androstenedione [1,2,6,7-^{3}H(N)]; dehydroepiandrosterone [1,2,6,7-^{3}H(N)]; dihydro-testosterone [1,2,4,5,6,7-^{3}H(N)]; 17β-estradiol [6,7-^{3}H(N)]; estrone [2,4,6,7-^{3}H(N)]; hydro-cortisone [1,2,6,7-^{3}H(N)]; progesterone [1,2,6,7-^{3}H(N)]; testosterone [1,2,6,7-^{3}H(N)]). All other chemicals and solvents were purchased from Sigma, Merck or AppliChem.

Cloning of AKR1B15 – The protein encoding sequences of the *AKR1B15* splice variants *AKR1B15.1* (Ensembl entry: *AKR1B15-201*, ENST00000423958) and *AKR1B15.2* (Ensembl entry: *AKR1B15-001*, ENST00000457545) were amplified by PCR from cDNA libraries of testis and thymus, respectively, using Phusion High Fidelity polymerase (NEB) and transcript specific primers with restriction enzyme sites (Table 1). The PCR products were cloned into pET28a(+) (Novagen) via *Nde I/Xho I*, into pcDNA3.1(+) (Invitrogen) via *Not I/Xho I*, into N-myc-pcDNA3 (modified pcDNA3, with N-terminal myc-tag) via *Not I/Xho I*, into pcDNA4-myc/HisB (Invitrogen) via *Hind III/Not I*, and into pIRES-hrGFP1α (Stratagene) via *Not I/Xho I* restriction sites, using *Hind III*, *Hind III*-HF, *Nde I*, *Not I*-HF, and *Xho I* restriction enzymes and T4 DNA Ligase (NEB). The complete sequence of the inserts was verified by Sanger sequencing. The sequences obtained were identical to the sequences deposited in the Ensembl database.

Expression and purification of AKR1B15 isoforms – His_6 tagged AKR1B15.1 and AKR1B15.2 were expressed in *E. coli* BL21 (DE3), carrying the respective pET28a(+) expression vectors, by induction with 0.5 mM IPTG and overnight incubation at 25 °C. Cell pellets were harvested, resuspended in lysis buffer (50 mM potassium phosphate buffer (KP_i) pH 8.0, 300 mM KCl, 5 mM imidazole, 1 % (m/v) N-lauroylsarcosine) and lysed by four cycles of 30 sec ultra-sonication pulses and 30 sec ice bath. The lysate was centrifuged (13000x*g*, 4 °C, 30 min), the resulting supernatant supplemented with TritonX100 to a final concentration of 2 % and applied on a Profinia Affinity Chromatography Protein Purification System (BioRad). The proteins were automatically purified according to the "Native IMAC Purification Protocol for His tagged Proteins" given by the manufacturer with modified buffers (2x wash buffer-1: 100 mM KP_i pH 8.0, 600 mM KCl, 10 mM imidazole, 0.5 % (m/v) N-lauroylsarcosine; 2x wash buffer-2: 100 mM KP_i pH 8.0, 600 mM KCl, 20 mM imidazole, 0.5 % (m/v) N-lauroylsarcosine; 2x elution buffer: 100 mM KP_i pH 8.0, 600 mM KCl, 500 mM imidazole, 0.1 % (m/v) N-lauroylsarcosine; 1x desalting buffer: 20 mM KP_i pH 7.4, 1 mM EDTA) using a 1 ml Bio-Scale Mini Profinity IMAC cartridge (BioRad) followed by a 10 ml Bio-Scale Mini Bio-Gel P-6 Desalting Cartridge (BioRad). The final concentration of eluted proteins was determined via BioRad DC Protein Assay Kit (BioRad).

Cell culture and transfection of human cells – HEK293 cells (CRL-1573™; ATCC) were cultured in DMEM (high glucose, stable glutamine) medium (PAA) and HeLa cells (ACC57; DSMZ) in MEM (L-glutamine) medium (PAA), both supplemented with 10 % FBS Gold (PAA), 100 U/ml penicillin, and 100 µg/ml streptomycin (Pen Strep; Gibco). BeWo cells (CCL-98™; ATCC) were cultured in F12-K medium (Invitrogen) supplemented with 10 % FBS Gold (PAA). SGBS cells were provided by Prof. M. Wabitsch (36) and cultured in DMEM/F-12 (1:1) (L-glutamine, 15 mM HEPES) medium (Gibco) supplemented with 10 % FBS Gold (PAA), 17 µM pantothenate, and 33 µM biotin. All cells were maintained at 37 °C, 5 % CO_2 in a humidified incubator and trypsinized for continuative cultivation or cell harvest using 0.05 % Trypsin-EDTA (Gibco). Transfections of HEK293 or HeLa cells were carried out using Xtreme DNA 9 transfection reagent (Roche) according to the manufacturer's protocols.

Enrichment of mitochondria from BeWo cells – Mitochondria were enriched from the BeWo cell line using a pump-controlled cell rupture system (PCC), following the protocol published by Schmitt *et al.* (37). For cell rupture $2x10^7$ freshly harvested BeWo cells were resuspended in 4 ml isolation buffer (300 mM sucrose, 5 mM Tes, and 200 µM EGTA, pH 7.2) and passed three times through a Cell Homogenizer with 10 µm clearance (Isobiotech) at a constant flow of 700 µl/min. Ruptured cells were centrifuged at 800x*g* and 4 °C for 5 min. The resulting supernatant was centrifuged once more at 9000x*g* and 4 °C for 10 min. The concentration of total protein in the fractions (800x*g* pellet, 9000x*g* pellet, and 9000x*g* supernatant) was determined via BioRad DC Protein Assay Kit (BioRad).

Generation of polyclonal and monoclonal antibodies against AKR1B15 – A peptide sequence with the most dissimilarity between AKR1B15 and AKR1B10 (Fig. 1B, red box) was used as antigen for the generation of polyclonal IgG antibodies against AKR1B15 in rabbit, which was carried out by 21st Century Biochemicals (Marlboro, MA). The peptide Ac-NWRAFDFKEFSHLC-amide was synthesized, conjugated to an immune carrier and used for the immunization of two rabbits to produce polyclonal antisera. Prior to use the resulting antibodies were affinity purified via the peptides deployed for immunization.

For the generation of the monoclonal antibody the peptide comprising the amino acid sequence QGFKTGDDFFPKDDKGNMISGKGTF from the human AKR1B15 protein (Fig. 1B, green box) was synthesized and coupled to ovalbumin (OVA) (Peps4LS, Heidelberg, Germany). Lou/c rats were immunized subcutaneously and intraperitoneally with a mixture of 50 µg peptide-OVA, 5 nmol CPG oligonucleotide (Tib Molbiol, Berlin), 500 µl PBS, and 500 µl incomplete Freund's adjuvant. A boost without adjuvant was given six weeks after the primary injection. Fusion of the myeloma cell line P3X63Ag8.653 (ATCC® CRL-1580™) with rat immune spleen cells was performed using standard procedures. Hybridoma supernatants

were tested in a differential ELISA with the biotinylated AKR1B15 peptide and an irrelevant biotinylated peptide on avidin coated ELISA plates. MAbs that reacted specifically with the AKR1B15 peptide were further analyzed by Western blot. Hybridoma culture supernatant of the anti-AKR1B15 clone 9A5 (rat IgG2a subclass) was used in this study.

SDS-PAGE and Western blotting – Denatured proteins were loaded onto a 12 % Mini-Protean or Criterion TGX gel (BioRad) and separated by conventional electrophoresis in running buffer (25 mM Tris pH 8.3, 192 mM glycine, 0.1 % (m/v) SDS). Afterwards gels were either stained via Coomassie Brilliant Blue (0.05 % (m/v) Coomassie Brilliant Blue R250, 10 % (v/v) acetic acid, 40 % (v/v) methanol) or blotted onto a PVDF membrane (Immobilon FL, Millipore) via semi-dry-blot in transfer-buffer (48 mM Tris, 39 mM glycine, 0.0375 % (m/v) SDS, 20 % (v/v) methanol). For testing antibody specificity, membranes after transfer were blocked with 5 % skimmed milk powder in PBS and then incubated overnight with primary antibodies in 0.5 % skimmed milk powder in PBS at 4 °C. Membranes were washed three times with PBS for 10 min, followed by incubation with HPR-conjugated secondary antibodies (also in 0.5 % skimmed milk powder in PBS) and another washing step. Signals were detected by incubating the membranes in Pierce ECL Plus Western Blotting Substrate (Thermo Scientific) according to the manufacturer's protocol and visualized using a Fusion FX7 system (Vilber Lourmat). A similar procedure was used to detect endogenous AKR1B15 isoforms, except that IR-dye labeled secondary antibodies and an Odyssey infrared imaging system (LI-COR) were used. Briefly, membranes were blocked with 50 % Odyssey Blocking Buffer (PBS) in PBS after transfer, antibodies were diluted in 50 % Odyssey Blocking Buffer (PBS) in PBS-T (0.05 % Tween20 in PBS), and washing steps were performed with PBS-T.

RNA isolation and cDNA synthesis – RNA from cultured cells was isolated using the RNeasy Mini Kit (Qiagen) combined with a DNaseI (Qiagen) digestion treatment. 1 µg RNA was reverse transcribed using Oligo$(dT)_{18}$ primers and the AffinityScript QPCR cDNA Synthesis Kit (Agilent) or AMV Reverse Transcriptase (Promega) according to the manufacturer's protocols.

RT-PCR and qPCR – End-point and real-time RT-PCR were carried out both with the same set of transcript specific primer pairs (Table 1). For the end-point RT-PCR, DreamTaq Green DNA Polymerase (Thermo) was used according to the manufacturer's protocol, with 38 amplification cycles for *AKR1B* transcripts and 24 cycles for *GAPDH* controls in a RoboCycler (Stratagene). PCR products were analyzed on a 2 % agarose gel containing 0.0025 % Midori Green (Biozym). QPCR was carried out applying the Perfect CT SYBR Green master mix (Quanta) and a 3-step-protocol (95 °C, 15 s; 57 °C, 30 s; 72 °C, 45 s) with an ABI 7900 HT instrument. Amplification efficiency was verified for each pair of primers using a standard curve constructed by serial dilution of a control template. Resulting C_T values for *AKR1B15.1*, *AKR1B15.2*, and *AKR1B10* transcripts were corrected by the average C_T value of the three housekeeping genes *GAPDH*, *HPRT*, and *18S RNA* (ΔC_T calculated) and normalized to the expression level of *AKR1B15.1* in placenta.

Activity assays – Catalytic activity was measured using ^{3}H-labeled steroids either with 10^6 harvested HEK293 cells (untransfected or transfected with pIRES-hrGFP-1α-AKR1B15) or with purified enzymes as described previously (38) with slight modifications. Reaction assays using HEK293 cells contained 10-40 nM ^{3}H-labeled steroid (Perkin Elmer, NEN) and generally 350 µM NAD(P)(H) cofactor (Serva, Sigma) in 500 µl reaction buffer (100 mM sodium phosphate buffer (NaP_i) pH 7.4, 1 mM EDTA). For the determination of Michaelis-Menten parameters 0-10 µM unlabeled steroid (Sigma) was added. In assay mixtures containing purified proteins (up to 55 nM), 0.05 % (m/v) BSA was added. The reaction mixtures were incubated with continuous shaking at 37 °C and the reaction was terminated by the addition of 20 % stop solution (0.5 M ascorbic acid, 1 % (v/v) acetic acid in methanol). Steroids were extracted on StrataC18-E (55 µm, 70 Å, 100 mg/ml) SPE cartridges (Phenomenex) with methanol as eluent. Substrates and products were separated by RP-HPLC on a Luna 5 µm C18(2) 125x4 mm column (Phenomenex) with 43 % ACN in MilliQ-H_2O as mobile phase, using a Beckman-Coulter system coupled to an online scintillation detector (Berthold LB506D).

Conversion of ^{3}H-labeled substrate was determined from ratios of areas under the peaks by Karat software (Beckman-Coulter).

Activity assays with unlabeled substrates were carried out with purified enzyme by measuring the change in NADPH absorbance at 340 nm using a Cary50 UV-Visible spectrophotometer (Varian) as described previously (2). The reaction mixture contained 150 µM NADPH, 6 µM purified enzyme, and substrate at variable concentrations (0-1 mM) in reaction buffer (100 mM NaP_i pH 7.0, 1 mM EDTA). The reaction was initiated by the addition of substrate to the pre-warmed mixture and allowed to run at 37 °C for 10-15 min with continuous absorbance recording. The initial velocity was calculated from the linear portion (0-5 min) of the curve. Kinetic parameters were calculated using SigmaPlot 12 software (Systat software).

Fluorescence titrations – The binding affinity of AKR1B15 isoforms to pyridine nucleotide cofactors was studied fluorometrically by following the quenching of the protein fluorescence (λ_{ex} = 280 nm, λ_{em} = 340 nm) upon addition of cofactors (39), using a Shimadzu RF5000 instrument. Aliquots containing 14 µg of purified protein (corresponding to a final concentration of 180 µM or 170 µM for AKR1B15.1 or AKR1B15.2, respectively) were added to 2 ml of 20 mM KP_i pH 7.4 at room temperature and equilibrated for 15-20 min. Aliquots of nucleotides were added sequentially and changes in emission were recorded. Dissociation constants were calculated by fitting Morrison equation [1] to the data after correction for the volume increase due to the addition of nucleotides and inner filter effect using SigmaPlot 12 software (Systat software).

$$\Delta F = \Delta F_{max} \cdot \frac{E+N+K_d-\sqrt{(E+N+K_d)^2-4\cdot E\cdot N}}{2\cdot E} \quad [1]$$

(ΔF, decrease in protein fluorescence; *E*, total enzyme concentration; *N*, total nucleotide concentration)

Subcellular localization studies – HeLa cells were grown on glass coverslips on the bottom of a 6-well plate and transiently transfected with plasmids (pcDNA3.1(+), N-myc-pcDNA3 or pcDNA4-myc/HisB backbone) encoding AKR1B15.1 or AKR1B15.2. For counterstaining the cytoplasm and endoplasmic reticulum, pCMV-DsRed-Express2 and pDsRed2-ER (Clontech) vectors were co-transfected, respectively. After transfection, cells were incubated at 37 °C and 5 % CO_2 in a humidified incubator for two additional days. Mitochondria were counterstained before the cells were prepared for immuno-cytochemical analysis by incubating living cells in serum-free MEM medium containing MitoTracker Orange CMTM-Ros (Molecular Probes) for 30 min. After staining the mitochondria, the cells were fixed in 3.7 % formaldehyde in PBS for 10 min at culturing conditions, permeabilized for 5 min using 0.5 % TritonX100 in PBS, and blocked with 3 % BSA in PBS for 1 h to prevent unspecific binding of the antibodies. The fixed cells were consecutively incubated with mouse-anti-myc (Roche) / goat-anti-rabbit-AlexaFluor 488 (Molecular Probes) antibodies in case of myc-tagged AKR1B15 isoforms or with rabbit-anti-AKR1B15 (21st Century Biochemicals) / goat-anti-rabbit-AlexaFluor 488 (Molecular Probes) and rat-anti-AKR1B15 clone 9A5 (in-house production) / goat-anti-rat-AlexaFluor 488 (Molecular Probes) in case of untagged proteins for 1-2 h. Before mounting objects on slides with VectaShield mounting medium (Vector Laboratories), nuclei were counterstained with Hoechst 33342 dye (Molecular Probes) diluted 1:5000 in PBS for 2 min. After each step, cells were washed twice with PBS. Subcellular localization data were collected and analyzed using a Zeiss AxioImager Z1/ApoTome confocal microscope with an AxioCam MRm camera and the AxioVision Rel. 4.8 software. *In silico* prediction of the localization of AKR1B15 isoforms were carried out using iPSORT (http://ipsort.hgc.jp) for non-plant proteins (40).

RESULTS

Two splice variants of AKR1B15 are expressed in vivo – Previously, we reported the identification and functional expression of a novel human member of the AKR1B family with 91 % amino acid identity to the well characterized human enzyme AKR1B10 (35). The gene encoding this protein, *AKR1B15*, is located on chromosome 7 next to *AKR1B10*. After our report, a newly predicted transcript sequence corresponding to the *AKR1B15* gene was deposited in the NCBI and Ensembl databases. The predicted transcript is

1621 bp in length and differs from our reported 1242 bp cDNA sequence in the 5'-end. Bioinformatics analysis revealed that the two sequences might result from an alternative use of the first exons of the *AKR1B15* gene, leading to two transcripts, in the following referred to as *AKR1B15.1* (Ensembl: transcript *AKR1B15-201*) for the short and *AKR1B15.2* (Ensembl: transcript *AKR1B15-001*) for the long transcript (Fig. 1A). To determine whether the alternative transcript *AKR1B15.2*, like *AKR1B15.1*, is expressed *in vivo*, we designed specific primers based on the predicted sequence, and amplified the corresponding product by PCR from the cDNA libraries of human thymus and salivary gland. Sequencing of the resulting product confirmed its 100 % identity to the sequence reported in the databases. Thus, *AKR1B15.2* mRNA is expressed in tissues and might be translated into a protein as it contains an open reading frame corresponding to a 344 amino acid protein. We conclude that the *AKR1B15* gene gives rise to two splice variants *in vivo*, presumably coding for two different protein isoforms (Fig. 1) and classify these protein isoforms as AKR1B15.1 (shorter, 316 amino acid isoform, encoded by transcript *AKR1B15.1*) and AKR1B15.2 (longer, 344 amino acid isoform, encoded by transcript *AKR1B15.2*) in accordance with the guidelines for the nomenclature of alternative splicing in the AKR superfamily (41). The two AKR1B15 isoforms differ in their N-termini, but share the same sequence beginning with the amino acid Ser23 in case of AKR1B15.1 and Ser51 in case of AKR1B15.2 (Fig. 1B). The four amino acid residues known to comprise the catalytic tetrad in AKRs are found in both AKR variants (Asp44, Tyr49, Lys78, and His111 for AKR1B15.1 and Asp72, Tyr77, Lys106, and His139 for AKR1B15.2, respectively; Fig. 1B).

Tissue distribution of AKR1B15 – To determine the tissue abundance of the two AKR1B15 isoforms, we first analyzed the expression of the two mRNA splice variants in a broad panel of tissues by RT-PCR, using transcript-specific primers as depicted in Fig. 1A (sequences listed in Table 1). For comparison, the expression of the highly homologous *AKR1B10* was analyzed in the same set of samples. We found that the expression of *AKR1B15.1* and *AKR1B15.2* differs completely from that of *AKR1B10*. While *AKR1B10* is expressed in a fairly ubiquitous manner across the tissue panel, the *AKR1B15* variants show more distinct distribution patterns (Fig. 2A). The highest expression levels of both *AKR1B15* splice variants were seen in adipose tissue, skeletal muscle, thymus, thyroid gland, and reproductive tissues (ovary, placenta, prostate, and testis). Corroborating the results from tissues, the human placental cell line BeWo and the pre-adipocyte cell strain SGBS express significant levels of both *AKR1B15* transcripts (Fig. 2A). In order to gain additional insights into the expression levels of *AKR1B15*, we performed qPCR on selected *AKR1B15* expressing tissues, using the same transcript-specific primers as for the end-point RT-PCR. We found the highest level of expression of both *AKR1B15* mRNA variants in placenta, followed by adipose tissue and testes (Fig. 2B). On the absolute level the abundance of *AKR1B15* mRNA was quite low. In placenta, the tissue with the highest level of expression, the abundance of *AKR1B15.1* transcripts was 100-150 -fold lower than that of *GAPDH*. In a majority of tissues the *AKR1B15.1* transcript was more abundant (at least 3-fold) than *AKR1B15.2*. In the thymus, prostate, and uterus comparable levels of both transcripts were found. Skeletal muscle was the only tissue where *AKR1B15.2* showed higher expression than *AKR1B15.1*. Only testis and adipose tissue displayed either of *AKR1B15* transcripts at a level of more than 10 % of that of *AKR1B15.1* in placenta. Skeletal muscle expressed around 2.5 % and all other tissues tested had less than 1 % of the level found in placenta. Hence, the expression pattern of *AKR1B15* is specific to a few tissues. *AKR1B10* and *AKR1B15*, despite high sequence similarity, display different tissue abundance: Among the tissues with *AKR1B15* expression, the abundance of *AKR1B10* mRNA exceeded that of *AKR1B15* by over 500-fold in the lung, thymus, and uterus. In contrast, the expression level of *AKR1B10* was only 6 % of that of *AKR1B15.1* in placenta (Fig. 2B).

Recombinant expression and purification of AKR1B15 – To verify that both *AKR1B15* mRNA variants produce functional proteins, we cloned their coding regions into the vector pET28a(+) and expressed encoded His-tagged proteins in *E. coli*. After induction with IPTG, bands with the predicted molecular weights were detected in bacterial extracts transformed with the corresponding constructs (Fig. 3A). AKR1B10, which differs only in 27 amino acid residues from AKR1B15.1 (Fig. 1B) was also expressed for

comparison. In contrast with AKR1B10, which is expressed as soluble protein in *E. coli*, both AKR1B15 isoforms were found in the insoluble fraction (Fig. 3B). We were able to solubilize both N-terminally histidine-tagged AKR1B15 isoforms using a sarkosyl-triton buffer system and purified both proteins to apparent homogeneity using a one-step immobilized metal (Ni^{2+}) affinity chromatography (Fig. 3C). We attributed the minor low molecular weight bands to the degradation or truncation products of AKR1B15 isoforms (Fig. 3C). The purification yielded 6-10 mg protein per liter bacterial culture.

Nucleotide binding – To determine the affinities of the two AKR1B15 proteins for nucleotide cofactors, we determined dissociation constants (K_d) of AKR1B15.1 and AKR1B15.2 for the four major pyridine nucleotides NADPH, NADH, $NADP^+$, and NAD^+ using fluorometric titrations. As shown in Fig. 4A, the addition of incremental concentrations of NADPH or $NADP^+$ to AKR1B15.1 led to a gradual decrease in protein fluorescence. The maximal degree of fluorescence quenching was 25-26 % in both cases, and the K_d values calculated from the concentration dependence of the decrease in fluorescence were: 59.3 ± 1.9 nM for NADPH and 60.4 ± 3.5 nM for $NADP^+$. In contrast, less than 3 % quenching of AKR1B15.1 fluorescence was observed with NADH and NAD^+ in concentrations of up to 40 µM after correction for inner filter effect (Fig. 4B; titration curve not shown). These results indicate that like other AKRs, AKR1B15.1 binds pyridine dinucleotides with high affinity and that it highly discriminates between phosphorylated and non-phosphorylated nucleotides. Addition of any of the four nucleotides to AKR1B15.2 failed to produce any change in protein fluorescence, in agreement with the lack of detectable enzymatic activity of AKR1B15.2 (see below).

Enzymatic activity of AKR1B15 isoforms – We performed detailed kinetic characterizations of both AKR1B15 isoforms, AKR1B15.1 and AKR1B15.2, using a variety of physiological substrates.

Because AKR1B15 is abundant in reproductive organs (the first full-length AKR1B15 transcript was initially found in testis) we reasoned that the protein might possess enzymatic activity with sex steroids. Therefore, we tested estrogens, androgens, progesterone, and corticosteroids as potential substrates of AKR1B15.1 or AKR1B15.2. In activity assays using HEK293 cells, transiently transfected with pIRES-hrGFP1α-AKR1B15.1 or pIRES-hrGFP1α-AKR1B15.2 and NADP(H) or NAD(H) as cofactor, we found that neither AKR1B15.1 nor AKR1B15.2 was able to reduce or oxidize progesterone and corticosteroids (data not shown). However, AKR1B15.1 catalyzed oxidation-reduction reactions with androgens and estrogens, as shown for the estrone and 17β-estradiol pair (Fig. 5A). Catalysis was supported by NADPH or $NADP^+$, but not by NADH or NAD^+ (up to a concentration of 1.5 mM), which agrees with the binding studies, suggesting that similar to a majority of other AKRs, AKR1B15 exhibits strong preference for phosphorylated cofactors. In addition, we found that AKR1B15.1 possesses high positional selectivity as it catalyzed only reactions on C17(β) position (C17) but not on C3 position (C3) of the steroid nucleus (Fig. 5B). In time-course experiments using purified AKR1B15.1 and estrogens as well as androgens in a final concentration of 20 nM, we found that AKR1B15.1 prefers reductive over oxidative reactions and androgens over estrogens (Fig. 5C). In contrast to AKR1B15.1, AKR1B15.2 did not exhibit any enzymatic activity with estrogens, androgens, or other steroids tested. Because neither the activity assays using solubilized purified AKR1B15.2 nor the assays using HEK293 cells, in which AKR1B15.2 was expressed under physiological conditions, showed any enzymatic activity, it appears that the protein is catalytically inactive and the lack of activity of the protein purified from bacteria could not be attributed to improper folding.

Because we found that AKR1B15.1 co-localizes with mitochondria (see below), we tested whether the enzyme displays catalytic activity with mitochondrial carbonyls or alcohols such as acetoacetyl-CoA, oxaloacetic acid, 2-oxobutyric acid, methylmalonyl-CoA, succinyl-CoA, DL-3-hydroxy-butyryl-CoA, and DL-3-hydroxy-3-methylglutaryl-CoA. We found that AKR1B15.1, but not AKR1B15.2, possessed enzymatic activity with acetoacetyl-CoA, while all other compounds were not detectably reduced or oxidized by either isoform (data not shown). These results indicate that AKR1B15.1 acts only on hydroxyl or keto groups of substrates possessing a bulky ring system like the steroid nucleus or the CoA.

We also determined kinetic parameters of AKR1B15.1 with different substrate classes using the purified enzyme (Table 2). The K_M values for oxidized steroids carrying a keto group on C17 appeared to be in the low micromolar range (1.9-2.8 µM), while reduced steroids carrying a hydroxyl group on C17 showed a 4-7 -fold higher K_M (7.1-19.2 µM). The turnover numbers (k_{cat} values) mirrored the results of the time course experiments: k_{cat} values of androgens (0.6-3.0 min^{-1}) were higher than those of estrogens (0.5-1.0 min^{-1}) and, with the exception of the k_{cat} of 3α,17β-androstandiol, k_{cat} values of reductive reactions were about 2-fold higher than those of oxidative reactions. Estimates of the catalytic efficiencies (k_{cat} / K_M) support the conclusion that the the protein has higher reductase than dehydrogenase activity. With acetoacetyl-CoA, the enzyme had a K_M value of 63.4 µM and a k_{cat} of 0.5 min^{-1}. The catalytic activity in the reverse direction, oxidation of 3-hydroxybutyryl-CoA, was below our detection limit (0.1 min^{-1}). AKR1B15.2 showed no activity with any of the substrates tested.

Generation of AKR1B15-specific antibodies and Western blot analysis – To examine the expression and the subcellular localization of AKR1B15 proteins, we first generated a specific polyclonal antibody that recognizes both AKR1B15 isoforms and distinguishes them from other AKR family members. Although the amino acid sequence of AKR1B15.1 is 91 % identical to that of AKR1B10, there is a single stretch of six consecutive amino acids at the C-terminus of the proteins (amino acids 299-304) that is different between the two proteins. Using a peptide corresponding to this area (AKR1B15.1: amino acids 295-307, AKR1B15.2: amino acids 323-335; Fig. 1B), we were able to generate a polyclonal antibody that recognized both AKR1B15.1 and AKR1B15.2, but did not cross-react with other recombinant human AKR proteins (Fig. 6A). This polyclonal antibody did not cross-react with AKR1B10 even when loading high amounts (200 ng) of purified protein (data not shown). In Western blot analysis of HEK293 transiently transfected with different plasmids encoding either AKR1B15.1 or AKR1B15.2, we could clearly detect the different overexpressed AKR1B15 isoforms. However, the polyclonal antibody also bound nonspecifically to other proteins of the HEK293 cells, including those having a similar molecular weight to the AKR1B15 isoforms (Fig. 6B, left panel). Because the high cross-reactivity of the polyclonal antibody could complicate the analysis of the expression of the native AKR1B15 proteins and because we found that antibodies against C-terminal sequences often cross-react with several other proteins, we generated a monoclonal antibody (rat-anti-AKR1B15 (9A5) recognizing both AKR1B15 isoforms and targeting a sequence more centrally located in the protein (AKR1B15.1: amino acids 114-138, AKR1B15.2: amino acids 142-166) with high divergence compared with AKR1B10 (Fig. 1B). Like the polyclonal antibody, the monoclonal antibody also recognized both AKR1B15.1 and AKR1B15.2 and did not cross-react with other recombinant human AKRs (Fig. 6A). In contrast with the polyclonal antibody, the monoclonal antibody displayed no cross-reactivity with proteins of the HEK293 cell background, when performing Western blots (Fig. 6B, right panel). To examine whether the mRNA of *AKR1B15* is translated to a protein *in vivo*, we performed Western blots of BeWo cell extracts using the specific monoclonal antibody and an IR-dye labeled secondary antibody (goat-anti-rat-AlexaFluor 790) which allows for the sensitive detection of low abundance proteins. Although no endogenous AKR1B15 isoforms were detectable in total cell lysates (data not shown), we were able to detect endogenous AKR1B15.1 and AKR1B15.2 in both the 800x*g* and the 9000x*g* pellet fraction of BeWo homogenates processed for the enrichment of mitochondria (Fig. 6C). Whereas AKR1B15.2 appeared as a single protein band at the expected molecular weight of 39.5 kDa, endogenous as well as overexpressed AKR1B15.1 was present as a double band corresponding to molecular weights of 36.5 kDa (expected) and 35.5-36 kDa, which could be proteolyzed or post-translationally modified form of the protein.

Subcellular localization of AKR1B15 isoforms – To characterize the two AKR1B15 isoforms in more detail, we determined their subcellular localization in the HeLa cell line overexpressing AKR1B15 isoforms using different constructs by immunocytochemistry. We found N- and C-terminally tagged AKR1B15.2 (expressed from N-myc-pcDNA3-AKR1B15.2 and pcDNA4-myc/HisB-AKR1B15.2, respectively) in the cytosol (Fig. 7-a, Fig. 7-c). A cytosolic localization was

observed also for AKR1B15.1, but only when fused to an N-terminal myc-tag (expressed from N-myc-pcDNA3-AKR1B15.1; Fig. 7-b). C-terminally tagged AKR1B15.1 (expressed from pcDNA4-myc/HisB-AKR1B15.1) co-localized with mitochondria (Fig. 7-d), indicating that the N-terminal amino acid sequence, which is different from that of AKR1B15.2, is important for the mitochondrial localization of AKR1B15.1. These results are in accord with theoretical analysis of AKR1B15 localization using the iPSORT prediction algorithm. The algorithm predicted a mitochondrial localization of AKR1B15.1 and a cytosolic localization of AKR1B15.2 when considering the N-terminal amino acid leader sequences Met1-Glu30 and Met1-Leu30, respectively. The mitochondrial localization of AKR1B15.1 (Fig. 7-f, Fig. 7-h) and cytosolic localization of AKR1B15.2 (Fig. 7-e, Fig. 7-g) was verified in HeLa cells transiently transfected with untagged AKR1B15.1 (pcDNA3.1(+)-AKR1B15.1) or AKR1B15.2 (pcDNA3.1(+)-AKR1B15.2) and stained with either the polyclonal rabbit-anti-AKR1B15 antibody or the monoclonal rat-anti-AKR1B15 antibody. Thus, AKR1B15.1 is the first AKR localized to the mitochondria.

DISCUSSION

In this work we demonstrate, that a novel human gene, *AKR1B15*, a member of the AKR super-family, is expressed in human tissues with the highest level found in reproductive organs, adipose tissue and skeletal muscle. In addition, we found that the *AKR1B15* gene undergoes alternative splicing producing two open reading frames corresponding to the protein isoforms AKR1B15.1 and AKR1B15.2. Both mRNA transcripts are expressed *in vivo*, although expression of both variants is limited in abundance and is not as ubiquitous as that of the highly homologous *AKR1B10*. For the most part, the transcript *AKR1B15-201* (referred to as *AKR1B15.1*, encoding protein AKR1B15.1) was more abundant than *AKR1B15-001* (referred to as *AKR1B15.2*, encoding protein AKR1B15.2) in tissues expressing both variants.

Using the monoclonal rat-anti-AKR1B15 (9A5) antibody, generated in house, we were able to show that both *AKR1B15* transcripts are translated into protein *in vivo*. Consistent with the low expression of mRNA, the abundance of the AKR1B15 protein was low as well; therefore, fractionation of subcellular components was necessary to detect the endogenous protein. Nevertheless, we were able to identify both endogenous AKR1B15 protein isoforms in the 800x*g* and 9000x*g* pellet of homogenates of the placental-derived BeWo cells, but were unable to detect endogenous AKR1B15 isoforms in commercial total protein human tissue lysates and total lysates of BeWo cells (data not shown). It appears that additional steps such as enrichment of subcellular components or immunoprecipitation will be necessary to characterize the expression of AKR1B15 in tissues and overcome its low abundance. Additionally, the detection of the proteins could be confounded by post-translational modifications which could reduce the affinity of the monoclonal antibody to the endogenous protein. Post-translational prediction algorithms indicated that both AKR1B15 isoforms could undergo various modifications (e.g., phosphorylation, SUMOylation, or ubiquitination) at several sites, including residues of the monoclonal antibody epitope (data not shown). These modifications could shift the apparent molecular of the proteins, destabilize the proteins or prevent antibody binding and thus interfere with the detection of endogenous AKR1B15 proteins. Additional research is required to investigate these possibilities.

Importantly, AKR1B15.1 showed enzymatic activity with sex steroids, both androgens and estrogens, and 3-keto-acyl-CoA thioesters, such as acetoacetyl-CoA. In contrast, AKR1B15.2 appeared to be an inactive enzyme, despite the fact that it possesses all four conserved amino acid residues of the catalytic tetrad (Asp72, Tyr77, Lys106, and His139). These findings are corroborated by the inability of AKR1B15.2 to bind nicotinamide adenine dinucleotide cofactors, whereas AKR1B15.1 binds NADPH and $NADP^+$ with an affinity in the nanomolar range. AKR1B15.1 displayed absolute specificity for phosphorylated dinucleotide cofactors, as neither binding nor activity has been observed with NADH or NAD^+.

Currently, it is difficult to distinguish whether the lack of nucleotide binding by AKR1B15.2 is due to improper folding or to an intrinsic property of

this protein. The undetectable enzymatic activity in both the artificial bacterial and the mammalian expression system, supports the latter hypothesis, suggesting that the long N-terminus influences the protein structure in a way that it prevents nucleotide and/or substrate access or binding. While the shorter AKR1B15 isoform, AKR1B15.1 like all other known AKR1B family members is 316 amino acids long, and shares 91 % amino acid sequence identity with AKR1B10, the AKR1B15.2 isoform displays greater differences because the N-terminus of AKR1B15.2 has no homology with other AKR1Bs and is 28 residues longer. In the crystal structure of AKR1B proteins the N-terminus folds into a hairpin of two β-sheets and creates a bottom of the $(\beta/\alpha)_8$ barrel (2, 42, 43). The alternative N-terminus in AKR1B15.2 substitutes the first 22 amino acid residues of other AKR1Bs, which might lead to a disarrangement of the bottom hairpin and the first β-sheet of the $(\beta/\alpha)_8$ barrel. This suggests the intriguing possibility that the N-terminus of AKR1B15.2 might serve as a modulatory domain, regulating access to the active site, by changing its conformation in response to protein modification such as phosphorylation. Alternatively, the non-homologous N-terminal loop of AKR1B15.2 may perform some additional function, analogous to the N-terminus of AKR6 family members (Kvβ proteins), which forms a "ball and chain" structure involved in the regulation of ion flow kinetics of voltage-gated potassium (Kv) channels (44, 45). Further investigation is needed to systematically address these possibilities.

Our measurements of enzymatic parameters show that AKR1B15.1 possesses K_M values in the low micromolar range for 17-keto-steroids, which are similar to the K_M values of other 17β-hydroxysteroid dehydrogenases (17β-HSDs), e.g., HSD17B1, HSD17B5, and HSD17B12 (46–48). We found that the enzyme is selective towards the carbonyl group located at the C17 position on the steroid nucleus. The comparatively low k_{cat} values observed with purified enzyme may result from the purification procedure, as AKR1B15.1 expressed in *E. coli* is an insoluble protein which needs to be reconstituted from inclusion bodies. In our k_{cat} calculations, we assumed that all protein molecules are properly folded, however, it is more likely that only a fraction of the purified enzyme is in the right conformation. Due to the high homology between AKR1B15.1 and AKR1B10 and the fact that estrogens and androgens are substrates of AKR1B15.1, we measured the activity of purified AKR1B10 with estrone, 17β-estradiol, Δ4-androstenedione, as well as testosterone. Although it is published that AKR1B10 is inhibited by steroids (49), we found that AKR1B10 is able to catalyze oxidation or reduction of those steroids in the nanomolar range, too. However, in contrast to AKR1B15, AKR1B10 preferentially catalyzed oxidative reactions of steroids (data not shown).

Our studies revealed that AKR1B15.1 is a predominantly reductive enzyme and that it co-localizes with mitochondria. The subcellular localization was surprising as most other human AKRs are cytosolic enzymes. Although *in silico* subcellular localization prediction is hypothetical and often does not agree with *in vivo* localization (50), iPSORT predicted a mitochondrial localization of AKR1B15.1 as well as a cytosolic localization of AKR1B15.2 and AKR1B10, which is in agreement with our results. The different behavior of AKR1B15.1 and AKR1B10 concerning localization can probably be explained by the different amino acid composition in their N-termini at positions 22 and 24. AKR1B15.1 possesses an arginine at position 22 and AKR1B10 features a lysine at this position, both of which have similar physicochemical properties. In contrast, the physicochemical properties of the amino acids at position 24 of AKR1B15.1 (Leu24) and AKR1B10 (Pro24) are clearly different. Several previous studies have shown that proline residues serve as a helix-breaker (51, 52). We therefore presume that Pro24 may be the amino acid responsible for different localization of AKR1B15.1 and AKR1B10. *In silico* prediction with iPSORT indicated a mitochondrial location of the AKR1B10 P24L mutant. This was confirmed in localization studies with N-terminal sequences fused to GFP, in which we were able to show that the substitution P24L in the N-terminus of AKR1B10 was sufficient to switch the subcellular localization of the respective GFP reporter construct from cytosolic to mitochondrial (data not shown). The results of Western blotting were consistent with the mitochondrial localization of AKR1B15.1, as endogenous AKR1B15.1 was detected in the 800x*g* and 9000x*g* pellets of BeWo cell homogenates. The 800x*g* pellet contains the nuclear fraction together with unbroken cells, cell debris and remains of the supernatant, whereas the

9000x*g* pellet represents the mitochondrial fraction (37). Surprisingly, AKR1B15.2 which seems localized to the cytosol by immunohistochemistry, was found mainly in the 9000x*g* pellet rather than the supernatant, suggesting strong association with subcellular organelles, possibly lysosomes, which are likely to be found in the 9000xg pellet (37).

Among the AKRs, only AKR7A2 has been suggested to be associated with mitochondria in SH-SY5Y neuroblastoma cells (53). However, its rat ortholog, AKR7A4, has also been reported localized to the Golgi apparatus (54), therefore the subcellular localization of this enzyme is still unclear. Hence, we conclude that we characterized the first AKR1 family member co-localizing with mitochondria; however, it still needs to be clarified whether AKR1B15.1 is located inside the mitochondria or strongly associated with the outer membrane.

Having established that AKR1B15.1 is localized to the mitochondria, we investigated whether mitochondria-specific carbonyls are potential substrates of the enzyme. We found that a 3-keto-acyl-CoA compound, acetoacetyl-CoA, can be reduced by AKR1B15.1 with a K_M of about 60 µM. We presume that AKR1B15.1 possesses low oxidizing activity with DL-3-hydroxy-butyryl-CoA, too, although the conversion could not be detected by our assays, probably due to limitations in the sensitivity of NADPH absorption; the readout of our assay. Longer chain 3-keto-acyl-CoAs, such as 3-keto-palmitoyl-CoA could also serve as substrates of AKR1B15.1. However, up to now we were unable to verify the proposed conversion due to limitations in substrate amounts and lack of sensitive and stable detection assays. Development of a more sensitive assay possibly based on product detection rather than nucleotide absorbance is necessary to confirm the reaction. The free oxo-(di)-carboxylic acids oxaloacetic acid and 2-oxobutyric acid, as well as the CoA-thioesters of dicarboxylic acids methylmalonyl-CoA and succinyl-CoA do not appear to be substrates of AKR1B15.1. This indicates that only carbonyl and not carboxyl groups can be reduced by AKR1B15.1. Moreover, it seems likely that all substrates need to possess a bulky ring backbone for their orientation in the substrate binding pocket of AKR1B15.1.

Although it might seem surprising that a single enzyme reduces such unrelated compounds as steroids and keto-acyl-CoA derivatives, it appears that many 17β-HSDs exhibit a wide substrate spectrum, which includes fatty acid derivatives, bile acids, and retinoids (55). The 17β-HSDs belong to two genetic superfamilies: aldo-keto reductases (AKRs) and short-chain dehydrogenases (SDRs) (56). To-date at least 14 types of 17β-HSDs have been identified, among which only type 5 belongs to the AKR superfamily (AKR1Cs). No activity with 3-keto-acyl-CoAs has been reported for AKR1C enzymes; however, 17β-HSDs of type 3, 4, 10, and 12, which belong to the SDR superfamily, possess activity with both steroids and keto-acyl-CoA conjugates (55). Therefore, we propose that although structurally a member of the AKR superfamily, AKR1B15.1 functionally is a 17β-hydroxysteroid dehydrogenase. Among the 17β-HSDs only one enzyme, HSD17B10, is mitochondrial and it catalyzes the NAD-dependent oxidoreduction of short-chain 3-keto-acyl-CoAs, along with sex steroids, as well as bile acid isomerization and glucocorticoid and gestagen catabolism (57). This enzyme is also called SCHAD (short-chain hydroxyl-acyl-CoA dehydrogenase) and it acts primarily in oxidative direction. Defects in this enzyme lead to hyper-insulinemic hypoglycemia (58, 59), abnormal thermogenesis and lower body weight in mice (60), as well as neural disorders such as Alzheimer's and Parkinson's diseases, mental retardation and infantile neuro-degeneration (61).

It could be argued that the results from the activity tests are somehow inconsistent with the subcellular localization of AKR1B15.1, because AKR1B15.1 preferably catalyzes reductive reactions, but the mitochondrial matrix has an oxidative environment, where among other reactions, β-oxidation of fatty acids and the very first steps of the steroid synthesis (from cholesterol to pregnenolone) take place (62). However, with the current data, the role of AKR1B15.1 in mitochondria can only be hypothesized. Different studies have shown that steroids and steroid receptors are present in mitochondria and affect their metabolism (63–65). One function of AKR1B15.1 may be the activation of the steroid signaling in mitochondria, as AKR1B15.1 catalyzes, among other reactions, the conversion of biologically low active estrone to

highly active 17β-estradiol, which binds to the mitochondrial estrogen receptor with high affinity (65). Like the nuclear genome, the mitochondrial genome contains hormone-responsive elements, e.g., the estrogen response element, regulating the expression of important ribosomal and structural proteins, as well as mitochondrially encoded proteins of the oxidative phosphorylation system (64, 66, 67). In addition, several studies have shown that 17β-estradiol protects the function of mitochondria in cells by reducing the amount of reactive oxygen species and therefore prevents cells from aging (64). Thus, AKR1B15.1 might provide the active steroid hormones which are known to reduce aging in mitochondria and cells. This hypothesis is supported by a recent publication by Yashin *et al.*, correlating a SNP in *AKR1B15* with longevity (68). Another function of AKR1B15.1 might relate to the reduction of 3-keto-acyl-CoAs, such as acetoacetyl-CoA. Reduction of 3-keto-acyl-CoAs is an important step in fatty acid synthesis although not expected in mitochondria, where the reverse process, the β-oxidation of fatty acids, takes place. However, several investigators have been able to show that *de novo* fatty acid synthesis (FAS) does occur in mitochondria via the FAS II pathway (69–71) and that components of the FAS II pathway might interact with the Complex I of the respiratory chain (72).

It has been recently reported that a naturally occurring mutation in *AKR1B15* gene (leading to an S8R mutation in AKR1B15.1, Fig. 1B) is linked to an infantile mitochondrial disease characterized by severe depletion of Complex I activity (73). Interactions between AKR1B15.1 and Complex I would explain why the mutation was associated with this infantile lethal phenotype (73). Here, direct protein-protein interactions in addition to the enzymatic activity of AKR1B15.1 might be of importance.

In conclusion, AKR1B15 is a novel member of the AKR superfamily with potential roles in steroid metabolism, regulation of the mitochondrial function and aging. Given the potential role of the enzyme in several key metabolic processes, further research is required to fully characterize its substrate specificity and mechanism, as well as its role in normal physiology and the significance of genetic polymorphisms in the development of pathological conditions, such as mitochondrial disease.

References

1. Penning, T. M., and Drury, J. E. (2007) Human aldo-keto reductases: Function, gene regulation, and single nucleotide polymorphisms. *Arch. Biochem. Biophys.* **464**, 241–250

2. Barski, O. A., Tipparaju, S. M., and Bhatnagar, A. (2008) The aldo-keto reductase superfamily and its role in drug metabolism and detoxification. *Drug Metab. Rev.* **40**, 553–624

3. Kondo, K. H., Kai, M. H., Setoguchi, Y., Eggertsen, G., Sjöblom, P., Setoguchi, T., Okuda, K. I., and Björkhem, I. (1994) Cloning and expression of cDNA of human delta 4-3-oxosteroid 5 beta-reductase and substrate specificity of the expressed enzyme. *Eur. J. Biochem.* **219**, 357–363

4. Fujii, Y., Watanabe, K., Hayashi, H., Urade, Y., Kuramitsu, S., Kagamiyama, H., and Hayaishi, O. (1990) Purification and characterization of rho-crystallin from Japanese common bullfrog lens. *J. Biol. Chem.* **265**, 9914–9923

5. Weng, J., Cao, Y., Moss, N., and Zhou, M. (2006) Modulation of voltage-dependent Shaker family potassium channels by an aldo-keto reductase. *J. Biol. Chem.* **281**, 15194–15200

6. Barski, O. A., Papusha, V. Z., Ivanova, M. M., Rudman, D. M., and Finegold, M. J. (2005) Developmental expression and function of aldehyde reductase in proximal tubules of the kidney. *Am. J. Physiol. Renal Physiol.* **289**, F200–F207

7. Penning, T. M. (2011) Human hydroxysteroid dehydrogenases and pre-receptor regulation: insights into inhibitor design and evaluation. *J. Steroid Biochem. Mol. Biol.* **125**, 46–56

8. Kabututu, Z., Manin, M., Pointud, J.-C., Maruyama, T., Nagata, N., Lambert, S., Lefrançois-Martinez, A.-M., Martinez, A., and Urade, Y. (2009) Prostaglandin F2alpha synthase activities of aldo-keto reductase 1B1, 1B3 and 1B7. *J. Biochem.* **145**, 161–168

9. Lemonde, H. A., Custard, E. J., Bouquet, J., Duran, M., Overmars, H., Scambler, P. J., and Clayton, P. T. (2003) Mutations in SRD5B1 (AKR1D1), the gene encoding delta(4)-3-oxosteroid 5beta-reductase, in hepatitis and liver failure in infancy. *Gut* **52**, 1494–1499

10. Lyon, R. C., Johnston, S. M., Watson, D. G., McGarvie, G., and Ellis, E. M. (2007) Synthesis and catabolism of gamma-hydroxybutyrate in SH-SY5Y human neuroblastoma cells: role of the aldo-keto reductase AKR7A2. *J. Biol. Chem.* **282**, 25986–25992

11. Srivastava, S., Chandra, A., Ansari, N. H., Srivastava, S. K., and Bhatnagar, A. (1998) Identification of cardiac oxidoreductase(s) involved in the metabolism of the lipid peroxidation-derived aldehyde-4-hydroxynonenal. *Biochem. J.* **329**, 469–475

12. Baba, S. P., Barski, O. A., Ahmed, Y., O'Toole, T. E., Conklin, D. J., Bhatnagar, A., and Srivastava, S. (2009) Reductive metabolism of AGE precursors: a metabolic route for preventing AGE accumulation in cardiovascular tissue. *Diabetes* **58**, 2486–2497

13. Guengerich, F. P., Cai, H., McMahon, M., Hayes, J. D., Sutter, T. R., Groopman, J. D., Deng, Z., and Harris, T. M. (2001) Reduction of aflatoxin B1 dialdehyde by rat and human aldo-keto reductases. *Chem. Res. Toxicol.* **14**, 727–737

14. Maser, E. (2004) Significance of reductases in the detoxification of the tobacco-specific carcinogen NNK. *Trends Pharmacol. Sci.* **25**, 235–237

15. Liu, S.-Q., Jin, H., Zacarias, A., Srivastava, S., and Bhatnagar, A. (2001) Binding of pyridine coenzymes to the beta-subunit of the voltage sensitive potassium channels. *Chem. Biol. Interact.* **130-132**, 955–962

16. Malup, T. K., Kobzev, V. F., Zhdanova, L. G., Slobodianiuk, Si., and Sviridov, S. M. (2000) [Analysis of nucleotide sequences in a region of S100b protein gene in AKR/J, DBA/dJ and BALB/cLac mice]. *Mol. Biol. (Mosk).* **34**, 366–367

17. Ramana, K. V. (2011) Aldose reductase: new insights for an old enzyme. *Biomol. Concepts* **2**, 103–114

18. Vikramadithyan, R. K., Hu, Y., Noh, H.-L., Liang, C.-P., Hallam, K., Tall, A. R., Ramasamy, R., and Goldberg, I. J. (2005) Human aldose reductase expression accelerates diabetic atherosclerosis in transgenic mice. *J. Clin. Invest.* **115**, 2434–2443

19. Gabbay, K. H. (2004) Aldose reductase inhibition in the treatment of diabetic neuropathy: where are we in 2004? *Curr. Diab. Rep.* **4**, 405–408

20. Dvornik, E., Simard-Duquesne, N., Krami, M., Sestanj, K., Gabbay, K. H., Kinoshita, J. H., Varma, S. D., and Merola, L. O. (1973) Polyol accumulation in galactosemic and diabetic rats: control by an aldose reductase inhibitor. *Science* **182**, 1146–1148

21. Kinoshita, J. H. (1990) A thirty year journey in the polyol pathway. *Exp. Eye Res.* **50**, 567–573

22. Bril, V., and Buchanan, R. A. (2006) Long-term effects of ranirestat (AS-3201) on peripheral nerve function in patients with diabetic sensorimotor polyneuropathy. *Diabetes Care* **29**, 68–72

23. Alexiou, P., Pegklidou, K., Chatzopoulou, M., Nicolaou, I., and Demopoulos, V. J. (2009) Aldose reductase enzyme and its implication to major health problems of the 21(st) century. *Curr. Med. Chem.* **16**, 734–752

24. Srivastava, S., Spite, M., Trent, J. O., West, M. B., Ahmed, Y., and Bhatnagar, A. (2004) Aldose reductase-catalyzed reduction of aldehyde phospholipids. *J. Biol. Chem.* **279**, 53395–53406

25. Vander Jagt, D. L., Robinson, B., Taylor, K. K., and Hunsaker, L. A. (1992) Reduction of trioses by NADPH-dependent aldo-keto reductases. Aldose reductase, methylglyoxal, and diabetic complications. *J. Biol. Chem.* **267**, 4364–4369

26. Srivastava, S., Vladykovskaya, E., Barski, O. A., Spite, M., Kaiserova, K., Petrash, J. M., Chung, S. S., Hunt, G., Dawn, B., and Bhatnagar, A. (2009) Aldose reductase protects against early atherosclerotic lesion formation in apolipoprotein E-null mice. *Circ. Res.* **105**, 793–802

27. Shinmura, K., Bolli, R., Liu, S.-Q., Tang, X.-L., Kodani, E., Xuan, Y., Srivastava, S., and Bhatnagar, A. (2002) Aldose reductase is an obligatory mediator of the late phase of ischemic preconditioning. *Circ. Res.* **91**, 240–246

28. Ramana, K. V, Chandra, D., Srivastava, S., Bhatnagar, A., Aggarwal, B. B., and Srivastava, S. K. (2002) Aldose reductase mediates mitogenic signaling in vascular smooth muscle cells. *J. Biol. Chem.* **277**, 32063–32070

29. Cao, D., Tat Fan, S., and Chung, S. S. M. (1998) Identification and characterization of a novel human aldose reductase-like gene. *J. Biol. Chem.* **273**, 11429–11435

30. Hyndman, D. J., and Flynn, T. G. (1998) Sequence and expression levels in human tissues of a new member of the aldo-keto reductase family. *Biochim. Biophys. Acta* **1399**, 198–202

31. Gallego, O., Belyaeva, O. V, Porté, S., Ruiz, F. X., Stetsenko, A. V, Shabrova, E. V, Kostereva, N. V, Farrés, J., Parés, X., and Kedishvili, N. Y. (2006) Comparative functional analysis of human medium-chain dehydrogenases, short-chain dehydrogenases/reductases and aldo-keto reductases with retinoids. *Biochem. J.* **399**, 101–109

32. Yoshitake, H., Takahashi, M., Ishikawa, H., Nojima, M., Iwanari, H., Watanabe, A., Aburatani, H., Yoshida, K., Ishi, K., Takamori, K., Ogawa, H., Hamakubo, T., Kodama, T., and Araki, Y. (2007) Aldo-keto reductase family 1, member B10 in uterine carcinomas: a potential risk factor of recurrence after surgical therapy in cervical cancer. *Int. J. Gynecol. Cancer* **17**, 1300–1306

33. Martin, H.-J., Breyer-Pfaff, U., Wsol, V., Venz, S., Block, S., and Maser, E. (2006) Purification and characterization of AKR1B10 from human liver: role in carbonyl reduction of xenobiotics. *Drug Metab. Dispos.* **34**, 464–470

34. Zhong, L., Shen, H., Huang, C., Jing, H., and Cao, D. (2011) AKR1B10 induces cell resistance to daunorubicin and idarubicin by reducing C13 ketonic group. *Toxicol. Appl. Pharmacol.* **255**, 40–47

35. Salabei, J. K., Li, X.-P., Petrash, J. M., Bhatnagar, A., and Barski, O. A. (2011) Functional expression of novel human and murine AKR1B genes. *Chem. Biol. Interact.* **191**, 177–184

36. Wabitsch, M., Brenner, R. E., Melzner, I., Braun, M., Möller, P., Heinze, E., Debatin, K. M., and Hauner, H. (2001) Characterization of a human preadipocyte cell strain with high capacity for adipose differentiation. *Int. J. Obes. Relat. Metab. Disord.* **25**, 8–15

37. Schmitt, S., Saathoff, F., Meissner, L., Schropp, E.-M., Lichtmannegger, J., Schulz, S., Eberhagen, C., Borchard, S., Aichler, M., Adamski, J., Plesnila, N., Rothenfusser, S., Kroemer, G., and Zischka, H. (2013) A semi-automated method for isolating functionally intact mitochondria from cultured cells and tissue biopsies. *Anal. Biochem.* **443**, 66–74

38. Mindnich, R., Haller, F., Halbach, F., Moeller, G., Hrabé de Angelis, M., and Adamski, J. (2005) Androgen metabolism via 17beta-hydroxysteroid dehydrogenase type 3 in mammalian and non-mammalian vertebrates: comparison of the human and the zebrafish enzyme. *J. Mol. Endocrinol.* **35**, 305–316

39. Barski, O. A., Gabbay, K. H., Grimshaw, C. E., and Bohren, K. M. (1995) Mechanism of human aldehyde reductase: characterization of the active site pocket. *Biochemistry* **34**, 11264–11275

40. Bannai, H., Tamada, Y., Maruyama, O., Nakai, K., and Miyano, S. (2002) Extensive feature detection of N-terminal protein sorting signals. *Bioinformatics* **18**, 298–305

41. Barski, O. A., Mindnich, R., and Penning, T. M. (2013) Alternative splicing in the aldo-keto reductase superfamily: implications for protein nomenclature. *Chem. Biol. Interact.* **202**, 153–158

42. Wilson, D. K., Bohren, K. M., Gabbay, K. H., and Quiocho, F. A. (1992) An unlikely sugar substrate site in the 1.65 A structure of the human aldose reductase holoenzyme implicated in diabetic complications. *Science* **257**, 81–84

43. Gallego, O., Ruiz, F. X., Ardèvol, A., Domínguez, M., Alvarez, R., de Lera, A. R., Rovira, C., Farrés, J., Fita, I., and Parés, X. (2007) Structural basis for the high all-trans-retinaldehyde reductase activity of the tumor marker AKR1B10. *Proc. Natl. Acad. Sci.* **104**, 20764–20769

44. McCormack, K., McCormack, T., Tanouye, M., Rudy, B., and Stühmer, W. (1995) Alternative splicing of the human Shaker K+ channel beta 1 gene and functional expression of the beta 2 gene product. *FEBS Lett.* **370**, 32–36

45. Pongs, O., and Schwarz, J. R. (2010) Ancillary subunits associated with voltage-dependent K+ channels. **90**, 755–796

46. Puranen, T. J., Poutanen, M. H., Peltoketo, H. E., Vihko, P. T., and Vihko, R. K. (1994) Site-directed mutagenesis of the putative active site of human 17 beta-hydroxysteroid dehydrogenase type 1. *Biochem. J.* **304**, 289–293

47. Byrns, M. C., Jin, Y., and Penning, T. M. (2011) Inhibitors of type 5 17β-hydroxysteroid dehydrogenase (AKR1C3): overview and structural insights. *J. Steroid Biochem. Mol. Biol.* **125**, 95–104

48. Luu-The, V., Tremblay, P., and Labrie, F. (2006) Characterization of type 12 17beta-hydroxysteroid dehydrogenase, an isoform of type 3 17beta-hydroxysteroid dehydrogenase responsible for estradiol formation in women. *Mol. Endocrinol.* **20**, 437–443

49. Endo, S., Matsunaga, T., Mamiya, H., Ohta, C., Soda, M., Kitade, Y., Tajima, K., Zhao, H.-T., El-Kabbani, O., and Hara, A. (2009) Kinetic studies of AKR1B10, human aldose reductase-like protein: endogenous substrates and inhibition by steroids. *Arch. Biochem. Biophys.* **487**, 1–9

50. Keller, B., Meier, M., and Adamski, J. (2009) Comparison of predicted and experimental subcellular localization of two putative rat steroid dehydrogenases from the short-chain dehydrogenase/reductase protein superfamily. *Mol. Cell. Endocrinol.* **301**, 43–46

51. Alías, M., Ayuso-Tejedor, S., Fernández-Recio, J., Cativiela, C., and Sancho, J. (2010) Helix propensities of conformationally restricted amino acids. Non-natural substitutes for helix breaking proline and helix forming alanine. *Org. Biomol. Chem.* **8**, 788–792

52. Lam, C.-W., Yuen, Y.-P., Cheng, W.-F., Chan, Y.-W., and Tong, S.-F. (2006) Missense mutation Leu72Pro located on the carboxyl terminal amphipathic helix of apolipoprotein C-II causes familial chylomicronemia syndrome. *Clin. Chim. Acta.* **364**, 256–259

53. Keenan, C., Ghaffar, S., Grant, A. W., Hinshelwood, A., Li, D., McGarvie, G., and Ellis, E. M. (2006) in *Enzymology and Molecular Biology of Carbonyl Metabolism. Vol. 12. West Lafayette* (Weiner, H., Plapp, B., Lindahl, R., and Maser, E., eds.) pp. 388–395, Purdue University Press

54. Kelly, V. P., Sherratt, P. J., Crouch, D. H., and Hayes, J. D. (2002) Novel homodimeric and heterodimeric rat gamma-hydroxybutyrate synthases that associate with the Golgi apparatus define a distinct subclass of aldo-keto reductase 7 family proteins. *Biochem. J.* **366**, 847–861

55. Mindnich, R., Möller, G., and Adamski, J. (2004) The role of 17 beta-hydroxysteroid dehydrogenases. *Mol. Cell. Endocrinol.* **218**, 7–20

56. Peltoketo, H., Luu-The, V., Simard, J., and Adamski, J. (1999) 17beta-hydroxysteroid dehydrogenase (HSD)/17-ketosteroid reductase (KSR) family; nomenclature and main characteristics of the 17HSD/KSR enzymes. *J. Mol. Endocrinol.* **23**, 1–11

57. Shafqat, N., Marschall, H.-U., Filling, C., Nordling, E., Wu, X.-Q., Björk, L., Thyberg, J., Mårtensson, E., Salim, S., Jörnvall, H., and Oppermann, U. (2003) Expanded substrate screenings of human and Drosophila type 10 17beta-hydroxysteroid dehydrogenases (HSDs) reveal multiple specificities in bile acid and steroid hormone metabolism: characterization of multifunctional 3alpha/7alpha/7beta/17beta/20beta/21-H. *Biochem. J.* **376**, 49–60

58. Clayton, P. T., Eaton, S., Aynsley-Green, A., Edginton, M., Hussain, K., Krywawych, S., Datta, V., Malingré, H. E. M., Berger, R., and van den Berg, I. E. T. (2001) Hyperinsulinism in short-chain L-3-hydroxyacyl-CoA dehydrogenase deficiency reveals the importance of beta-oxidation in insulin secretion. *J. Clin. Invest.* **108**, 457–465

59. Heslegrave, A. J., and Hussain, K. (2013) Novel insights into fatty acid oxidation, amino acid metabolism, and insulin secretion from studying patients with loss of function mutations in 3-hydroxyacyl-CoA dehydrogenase. *J. Clin. Endocrinol. Metab.* **98**, 496–501

60. Schulz, N., Himmelbauer, H., Rath, M., van Weeghel, M., Houten, S., Kulik, W., Suhre, K., Scherneck, S., Vogel, H., Kluge, R., Wiedmer, P., Joost, H.-G., and Schürmann, A. (2011) Role of medium- and short-chain L-3-hydroxyacyl-CoA dehydrogenase in the regulation of body weight and thermogenesis. *Endocrinology* **152**, 4641–4651

61. Yang, S.-Y., He, X.-Y., and Schulz, H. (2005) 3-Hydroxyacyl-CoA dehydrogenase and short chain 3-hydroxyacyl-CoA dehydrogenase in human health and disease. *FEBS J.* **272**, 4874–4883

62. Miller, W. L., and Auchus, R. J. (2011) The molecular biology, biochemistry, and physiology of human steroidogenesis and its disorders. *Endocr. Rev.* **32**, 81–151

63. Yang, S.-H., Liu, R., Perez, E. J., Wen, Y., Stevens, S. M., Valencia, T., Brun-Zinkernagel, A.-M., Prokai, L., Will, Y., Dykens, J., Koulen, P., and Simpkins, J. W. (2004) Mitochondrial localization of estrogen receptor beta. *Proc. Natl. Acad. Sci. U. S. A.* **101**, 4130–4135

64. Vasconsuelo, A., Milanesi, L., and Boland, R. (2013) Actions of 17β-estradiol and testosterone in the mitochondria and their implications in aging. *Ageing Res. Rev.* **12**, 907–917

65. Pedram, A., Razandi, M., Wallace, D. C., and Levin, E. R. (2006) Functional estrogen receptors in the mitochondria of breast cancer cells. *Mol. Biol. Cell* **17**, 2125–2137

66. Demonacos, C., Djordjevic-Markovic, R., Tsawdaroglou, N., and Sekeris, C. E. (1995) The mitochondrion as a primary site of action of glucocorticoids: the interaction of the glucocorticoid receptor with mitochondrial DNA sequences showing partial similarity to the nuclear glucocorticoid responsive elements. *J. Steroid Biochem. Mol. Biol.* **55**, 43–55

67. Demonacos, C. V, Karayanni, N., Hatzoglou, E., Tsiriyiotis, C., Spandidos, D. A., and Sekeris, C. E. (1996) Mitochondrial genes as sites of primary action of steroid hormones. *Steroids* **61**, 226–232

68. Yashin, A. I., Wu, D., Arbeev, K. G., and Ukraintseva, S. V (2010) Joint influence of small-effect genetic variants on human longevity. *Aging (Albany. NY).* **2**, 612–620

69. Witkowski, A., Joshi, A. K., and Smith, S. (2007) Coupling of the de novo fatty acid biosynthesis and lipoylation pathways in mammalian mitochondria. *J. Biol. Chem.* **282**, 14178–14185

70. Hiltunen, J. K., Schonauer, M. S., Autio, K. J., Mittelmeier, T. M., Kastaniotis, A. J., and Dieckmann, C. L. (2009) Mitochondrial fatty acid synthesis type II: more than just fatty acids. *J. Biol. Chem.* **284**, 9011–9015

71. Parl, A., Mitchell, S. L., Clay, H. B., Reiss, S., Li, Z., and Murdock, D. G. (2013) The mitochondrial fatty acid synthesis (mtFASII) pathway is capable of mediating nuclear-mitochondrial cross talk through the PPAR system of transcriptional activation. *Biochem. Biophys. Res. Commun.* **441**, 418–424

72. Schulte, U. (2001) Biogenesis of respiratory complex I. *J. Bioenerg. Biomembr.* **33**, 205–212

73. Calvo, S. E., Compton, A. G., Hershman, S. G., Lim, S. C., Lieber, D. S., Tucker, E. J., Laskowski, A., Garone, C., Liu, S., Jaffe, D. B., Christodoulou, J., Fletcher, J. M., Bruno, D. L., Goldblatt, J., DiMauro, S., Thorburn, D. R., and Mootha, V. K. (2012) Molecular diagnosis of infantile mitochondrial disease with targeted next-generation sequencing. *Sci. Transl. Med.* **4**, 118ra10

Acknowledgments - The authors are grateful to Anna Rast, Aurelia Weber and Xiao-Ping Li for their excellent technical assistance as well as Dr. Janina Tokarz for reading the manuscript. We also thank Dr. Margarita Ivanova for initial immunocytochemistry work and helpful discussions as well as Sabine Schmitt for her expertise in the enrichment of mitochondria.

FOOTNOTES

*This work was supported in part by National Institutes of Health Grants HL55477, HL59378, and GM103492.

[1]To whom correspondence may be addressed:
Oleg A. Barski, NIGMS, NIH, 45 Center Dr. Rm. 2AS55C, Bethesda, MD 20892, USA. Tel: (301)-496-1511; Fax: (301)-480-2802; E-mail: oleg.barski@nih.gov (present address).
Disclaimer: This article was prepared while Oleg A. Barski was employed at the University of Louisville. The opinions expressed in this article are the author's own and do not reflect the view of the National Institutes of Health, the Department of Health and Human Services, or the United States government.
or
Jerzy Adamski , Helmholtz Zentrum Muenchen, German Research Center for Environmental Health, Institute of Experimental Genetics, Genome Analysis Center, Ingolstaedter Landstr. 1, 85764 Neuherberg, Germany. Tel.: 049-89-3187-3155; Fax: 049-89-3187-3225; E-mail: Adamski@helmholtz-muenchen.de

[2]The abbreviations used are:
A-diol, 3α,17β-androstandiol; A-dione, androstanedione; AKR, aldo-keto reductase; AN, androsterone; D4-AE, Δ4-androstenedione; DHEA, dehydroepiandrosterone; DHT, dihydrotestosterone; E1, estrone; E2, 17β-estradiol; ER, endoplasmic reticulum; FAS, fatty acid synthesis; HSD, hydroxysteroid dehydrogenase; KP_i, potassium phosphate buffer; NaP_i, sodium phosphate buffer; RT, reverse transcriptase; SD, standard deviation; SE, standard error; T, testosterone.

FIGURE LEGENDS

FIGURE 1: Comparison of *AKR1B10* and *AKR1B15* on gene, transcript, and protein level.
(A) Schematic illustrations of intron-exon structures of *AKR1B10* and *AKR1B15*. Alternative use of exons in the 5'-region of AKR1B15 generates two splice variants, referred to as *AKR1B15.1* (Ensembl transcript: *AKR1B15-201*) and *AKR1B15.2* (Ensembl transcript: *AKR1B15-001*), which are translated into the protein isoforms AKR1B15.1 and AKR1B15.2, respectively. Black straight lines depict introns, while exons are shown as numbered rectangles. Translated exons of *AKR1B10* are colored in green, alternatively spliced exons in the 5'-region of *AKR1B15* are colored orange (for *AKR1B15.1*) or yellow (for *AKR1B15.*2) followed by orange-yellow-striped common exons. UTR's are shown in white. Arrows depict annealing sites for transcript specific primer pairs: AKR10-15.1-fwd (a), AKR15.2-fwd (b), AKR15-rev (c), AKR10-rev (d). **(B)** Alignment of the protein sequences of AKR1B10, AKR1B15.1, and AKR1B15.2. Alternative splicing of the 5'- region of AKR1B15 leads to a totally different and longer N-terminus of AKR1B15.2 compared with that of AKR1B15.1. AKR1B15.1 and AKR1B10 possess high homology in their N-termini. Amino acids of the catalytic tetrad are highlighted in bold, the serine at position 8 of AKR1B15.1, which is mutated in a phenotype with a mitochondrial disease, is colored in blue, and the proline at position 24 of AKR1B10, which is responsible for its cytosolic localization, is colored in green. The recognition region for the monoclonal rat-anti-AKR1B15 antibody is highlighted by a green box; the C-terminal recognition region for the polyclonal rabbit-anti-AKR1B15 antibody is highlighted by a red box.

FIGURE 2: Expression of *AKR1B10*, *AKR1B15.1*, and *AKR1B15.2* in tissues and cell lines.
(A) Semi-quantitative end-point RT-PCR with cDNA from tissues and cell lines shows different expression patterns for *AKR1B15* and *AKR1B10*. *GAPDH* as well as reactions without reverse transcriptase (no RT) or cDNA (H_2O) serve as controls. **(B)** Quantitative real-time PCR with cDNA of selected tissues validate differences in expression levels of *AKR1B15.1*, *AKR1B15.2*, and *AKR1B10*. Expression levels of *AKR1B15.1* (black bars), *AKR1B15.2* (gray bars), and *AKR1B10* (open bars) transcripts are shown on a logarithmic scale and are normalized to the expression of *AKR1B15.1* in placenta after correction of the C_T values by the average of the three housekeeping genes: *GAPDH*, *HPRT*, and *18S RNA*; error bars represent standard deviations from two independent cDNA sets.

FIGURE 3: Expression and purification of AKR1B10, AKR1B15.1, and AKR1B15.2 in *E. coli* BL21 (DE3). Protein bands in Coomassie stained SDS-polyacrylamide gels are shown.
(A) Lysates of IPTG-induced (I) but not uninduced (U) cell pellets show clear bands of AKR1B10, AKR1B15.1, and AKR1B15.2, respectively. **(B)** After centrifugation of induced cell lysates both AKR1B15 isoforms show up as insoluble proteins in the pellet fraction (P), while AKR1B10 is soluble and therefore present in the supernatant (SN). **(C)** Purification of AKR1B15.1 and AKR1B15.2 leads to sufficiently pure protein, containing only minute amounts of degradation or truncation products.

FIGURE 4: Binding of dinucleotide cofactors to AKR1B15.1.
(A) NADPH (open circles) -, or $NADP^+$ (filled circles) - dependent decline in the fluorescence of AKR1B15.1 measured in 20 mM KP_i buffer pH 7.4 using an excitation wavelength of 280 nm and emission wavelength of 340 nm. Data are shown as discrete points and curves are best fits of equation [1] to the data. Changes in fluorescence were normalized to the value of the initial fluorescence of the protein; data are presented as mean ± SD of two independent measurements. **(B)** Parameters gained from cofactor titration studies. K_d and maximum quenching (ΔF_{max}) were calculated from the fluorescence curves by fitting equation [1] to the data.

FIGURE 5: AKR1B15.1 catalyzes redox reactions with steroids.
(A) AKR1B15.1 exhibits strong preference for phosphorylated cofactor by catalyzing redox reactions only in the presence of NADP(H) but not NAD(H). Activity tests were carried out using 10^6 HEK293 cells either non-transfected (HEK293) or transiently transfected with pIRES-hrGFP-1α-AKR1B15.1 (HEK293+AKR1B15.1), 15 nM ^{3}H-labeled estrone or 10 nM ^{3}H-labeled 17β-estradiol, and 350 µM cofactor in reaction buffer. Bars represent the mean of steroid conversion in % after 60 min (for estrone) and 120 min (for 17β-estradiol) incubation; error bars show standard deviations of three replicates. **(B)** AKR1B15.1 possesses activity on the C17 β-position of the steroid nucleus (C17) but not on the C3 position (C3). Activity tests were carried out using 10^6 HEK293 cells transiently transfected with pIRES-hrGFP-1α-AKR1B15.1, 10 to 40 nM ^{3}H-labeled steroids, and 350 µM NADPH (+ NADPH) or $NADP^+$ (+ $NADP^+$) cofactor in reaction buffer. Bars represent conversion in %. **(C)** Comparison of reaction velocities with different steroids. Activity tests were carried out using 90 nM purified AKR1B15.1, 20 nM (corresponding to 10 pmol per reaction) ^{3}H-labeled steroids, and 300-325 µM cofactors in reaction buffer. Results of reductive reactions using NADPH are represented by open symbols, those of oxidative reactions using $NADP^+$ by filled symbols. Data represent mean ± SD (n=3).

FIGURE 6: Generation of specific polyclonal and monoclonal anti-AKR1B15 antibodies and detection of endogenous AKR1B15 isoforms.
(A) Different His-tagged human AKRs (AKR6A3, AKR1B1, AKR1B10, AKR1B15.1, AKR1B15.2, and AKR1A1) were expressed in *E. coli* BL21 (DE3) and analyzed by Western blot using polyclonal rabbit-anti-AKR1B15, monoclonal rat-anti-AKR1B15 (9A5) or polyclonal rabbit-anti-His-tag (Cell Signaling) antibodies as primary antibodies and HRP-conjugated goat-anti-rabbit (Life Technologies) and mouse-anti-rat-IgG2A (in-house production) secondary antibodies. Non-transformed *E. coli* BL21 (DE3) served as negative control. The anti-His-tag staining showed that all proteins were expressed (lower panel). **(B)** Untagged AKR1B15.1 and AKR1B15.2 were overexpressed in HEK293 cells and analyzed by Western blot using polyclonal rabbit-anti-AKR1B15 and monoclonal rat-anti-AKR1B15 (9A5) antibodies as primary antibodies and goat-anti-rabbit (Life Technologies) and mouse-anti-rat-IgG2A (in-house production) antibodies as HRP-conjugated secondary antibodies, respectively. Non-transfected HEK293 cells served as negative control. While the polyclonal antibody is fairly unspecific, as it recognizes several proteins, the monoclonal antibody shows high specificity to both AKR1B15 isoforms with no cross-reactivity. **(C)** Fractions (800x*g* and 9000x*g* pellets) of the enrichment of mitochondria from BeWo cells were analyzed for the presence of endogenous AKR1B15 isoforms by Western blot using monoclonal rat-anti-AKR1B15 (9A5) antibody as primary and IR-dye conjugated goat-anti-rat-AlexaFluor 790 (Dianova) antibody as secondary. A mixture of extracts from HEK293 cells overexpressing untagged AKR1B15.1 or AKR1B15.2 served as a positive control and non-transfected HEK293 cells as well as a secondary antibody only hybridization (left panel) served as negative controls. Endogenous AKR1B15.1 is marked by an asterisk and AKR1B15.2 by an arrowhead.

FIGURE 7: Subcellular distribution of the two AKR1B15 isoforms.
HeLa cells were transiently transfected with either N-myc-pcDNA3-AKR1B15.2 **(a)**, N-myc-pcDNA3-AKR1B15.1 **(b)**, pcDNA4-myc/His B-AKR1B15.2 **(c)**, pcDNA4-myc/His B-AKR1B15.1 **(d)**, pcDNA3.1(+)-AKR1B15.2 **(e, g)**, or pcDNA3.1(+)-AKR1B15.1 **(f, h)** in order to overexpress N-terminally myc-tagged (a, b), C-terminally myc-tagged (c, d), or untagged (e-h) protein. Nuclei were stained using Hoechst 33342 dye **(A)**; mitochondria were stained using Mito-Tracker Orange CMTM-Ros **(B)**; myc-tagged AKR1B15.1 or AKR1B15.2 were stained using mouse-anti-myc / goat-anti-mouse-AlexaFluor 488 antibodies and untagged AKR1B15.1 was stained using polyclonal rabbit-anti-AKR1B15 / goat-anti-rabbit-AlexaFluor 488 antibodies or monoclonal rat-anti-AKR1B15 / goat-anti-rat-AlexaFluor 488 antibodies **(C)**. The individual staining as well as the overlays **(D)** demonstrate that AKR1B15.2 is a cytoplasmic protein, while C-terminally myc-tagged AKR1B15.1 as well as untagged

AKR1B15.1 co-localize with mitochondria. Nuclei are shown in blue, mitochondria in red, AKR1B15 in green, and co-localization in yellow.

TABLE 1:
Primer names and sequences used for cloning and semi-quantitative RT-PCR (RT) or qPCR (Q).
Restriction sites are underlined and coding sequences are shown in capital letters.

primers for cloning into pET28a(+):		
AKR1B15.1-*Nde*I_fwd:	5'-cccttccatATGGCCACGTTTGTGGAGCT-3'	
AKR1B15.2-*Nde*I_fwd:	5'-tcaagctacatATGGTCTTACAAATGGAA-3'	
AKR1B15-*Xho*I_rev (1)	5'-agatcctcgagTCAATATTCTGCATCGAA-3'	
primers for cloning into pcDNA3.1(+)		
AKR1B15.1-*Not*I_fwd (1):	5'-aagaagcggccgcaccATGGCCACGTTTGTGGAGCT-3'	
AKR1B15.2-*Not*I_fwd (1):	5'-aagaagcggccgcaccATGGTCTTACAAATGGA-3'	
AKR1B15-*Xho*I_rev (1):	5'-agatcctcgagTCAATATTCTGCATCGAA-3'	
primers for cloning into N-myc-pcDNA3		
AKR1B15.1-*Not*I_fwd (2):	5'-ttttgcggccgcaaGCCACGTTTGTGGAGCTC-3'	
AKR1B15.2-*Not*I_fwd (2):	5'-ttttgcggccgcaaGTCTTACAAATGGAACCCCA-3'	
AKR1B15-*Xho*I_rev (2):	5'-tttctcgagTCAATATTCTGCATCGAAGGGAAAGT-3'	
primers for cloning into pcDNA4-myc/HisB		
AKR1B15.1-*Hind*III_fwd:	5'-ttttaagcttATGGCCACGTTTGTGGAGCTC-3'	
AKR1B15.2-*Hind*III_fwd:	5'-ttttaagcttATGGTCTTACAAATGGAACCCCA-3'	
AKR1B15-*Not*I_rev:	5'-ttttgcggccgctATATTCTGCATCGAAGGGAAAGT-3'	
primers for cloning into pIRES-hrGFP-1α		
pET28-AKR1B15.1-*Not*I_fwd:	5'-aagaagcggccgcaccATGGGCAGCAGCCAT-3'	
AKR1B15.2-*Not*I-His_fwd:	5'-aaatggcggccgcaccatgggcagcagccatcatcatcatcacagcagcggcctggtgc--cggcggcagccatATGGTCTTACAAATGGAACCCCAAGTGAACTCA-3'	
AKR1B15-*Xho*I_rev (1):	5'-agatcctcgagTCAATATTCTGCATCGAA-3'	
primers for RT-PCR (RT) and qPCR (Q)		
AKR10-15.1_fwd:	5'-CCACGTTTGTGGAGCTCAGT-3'	(RT, Q)
AKR15.2_fwd:	5'-CCCTTTGACTGGCCTAAAGA-3'	(RT, Q)
AKR10_rev:	5'-AACGTTGCTTTTCCACCGATGGC-3'	(RT, Q)
AKR15_rev:	5'-AACGTTCCTTTTCCACTGATCAT-3'	(RT, Q)
GAPDH_fwd (1):	5'-AGTCAACGGATTTGGTCGTA-3'	(RT)
GAPDH_rev (1):	5'-ATGACAAGCTTCCCGTTCT-3'	(RT)
GAPDH_fwd (2):	5'-GGTGGTCTCCTCTGACTTCAACA-3'	(Q)
GAPDH_rev (2):	5'-GTTGCTGTAGCCAAATTCGTTGT-3'	(Q)
HPRT1:	RT^2 qPCR Primer Assay for Human HPRT1 (SABiosciences)	(Q)
18S-RNA:	RT^2 qPCR Primer Assay for Human 18SrRNA (SABiosciences)	(Q)

TABLE 2: Kinetic parameters of AKR1B15.1.
Kinetic parameters of AKR1B15.1 were determined with purified enzyme and cofactor NADPH (300 µM) for reductive reactions or $NADP^+$ (325 µM) for oxidative reactions. K_M and k_{cat} values were calculated by Michaelis-Menten fit (SigmaPlot) of initial reaction velocities measured with increasing concentrations of either unlabeled steroids, spiked with 10 pmol ^{3}H-labeled steroids, or unlabeled acetoacetyl-CoA.
K_M, Michaelis constant; k_{cat}, turnover number; k_{cat} / K_M, catalytic efficiency. Values are mean ± SE (n=3).

	substrate	K_M [µM]	k_{cat} [min^{-1}]	k_{cat} / K_M [μM^{-1} min^{-1}]
reductive reactions	androsterone	2.8 ± 0.2	1.7 ± 0.1	0.61
	Δ4-androstenedione	1.9 ± 0.2	1.1 ± 0.1	0.60
	estrone	2.5 ± 0.4	1.0 ± 0.1	0.38
	acetoacetyl-CoA	63.4 ± 7.4	0.5 ± 0.1	0.01
oxidative reactions	3α,17β-androstandiol	19.2 ± 2.3	3.0 ± 0.3	0.16
	testosterone	7.1 ± 1.5	0.6 ± 0.1	0.09
	17β-estradiol	9.1 ± 1.2	0.5 ± 0.1	0.06

Figure 1:

A

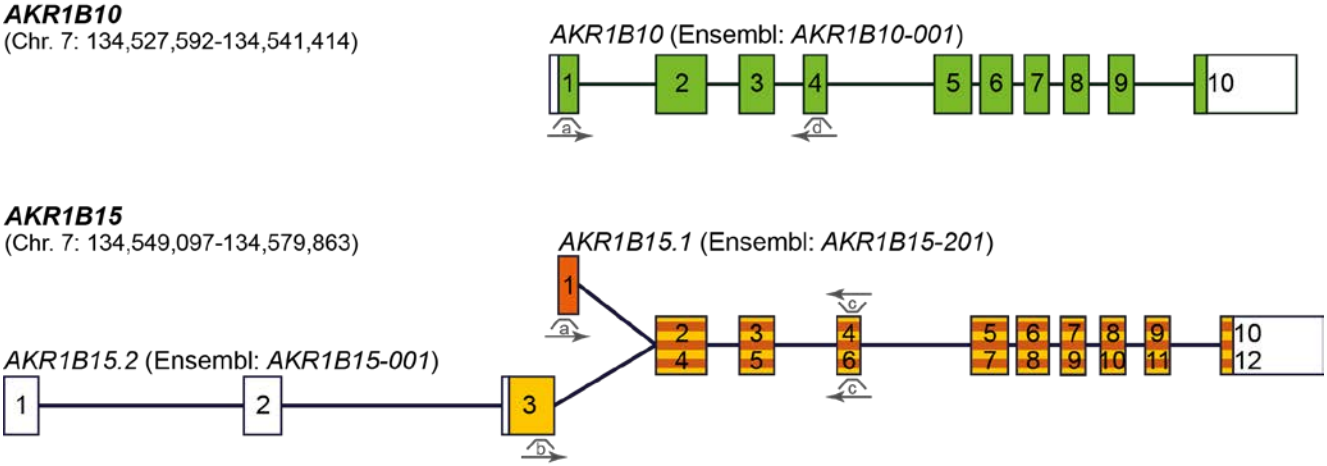

B

```
AKR1B10      1  ----MATFVELS--------TKAKMPIVGLGT----------WK----SPLGKVKEAV   32
AKR1B15.1    1  ----MATFVELS--------TKAKMPIVGLGT----------WR----SLLGKVKEAV   32
AKR1B15.2    1  MVLQMEPQVNSTNNFHQGPLDQPVGPLTGLKSSLLKDTTSAGPLLRPYPASLLGKVKEAV   60

AKR1B10     33  KVAIDAGYRHIDCAYVYQNEHEVGEAIQEKIQEKAVKREDLFIVSKLWPTFFERPLVRKA   92
AKR1B15.1   33  KVAIDAEYRHIDCAYFYENQHEVGEAIQEKIQEKAVMREDLFIVSKVWPTFFERPLVRKA   92
AKR1B15.2   61  KVAIDAEYRHIDCAYFYENQHEVGEAIQEKIQEKAVMREDLFIVSKVWPTFFERPLVRKA  120

AKR1B10     93  FEKTLKDLKLSYLDVYLIHWPQGFKSGDDLFPKDDKGNAIGGKATFLDAWEAMEELVDEG  152
AKR1B15.1   93  FEKTLKDLKLSYLDVYLIHWPQGFKTGDDFFPKDDKGNMISGKGTFLDAWEAMEELVDEG  152
AKR1B15.2  121  FEKTLKDLKLSYLDVYLIHWPQGFKTGDDFFPKDDKGNMISGKGTFLDAWEAMEELVDEG  180

AKR1B10    153  LVKALGVSNFSHFQIEKLLNKPGLKYKPVTNQVECHPYLTQEKLIQYCHSKGITVTAYSP  212
AKR1B15.1  153  LVKALGVSNFNHFQIERLLNKPGLKYKPVTNQVECHPYLTQEKLIQYCHSKGITVTAYSP  213
AKR1B15.2  181  LVKALGVSNFNHFQIERLLNKPGLKYKPVTNQVECHPYLTQEKLIQYCHSKGITVTAYSP  240

AKR1B10    213  LGSPDRPWAKPEDPSLLEDPKIKEIAAKHKKTAAQVLIRFHIQRNVIVIPKSVTPARIVE  272
AKR1B15.1  213  LGSPDRPWAKPEDPSLLEDPKIKEIAAKHKKTTAQVLIRFHIQRNVTVIPKSMTPAHIVE  272
AKR1B15.2  241  LGSPDRPWAKPEDPSLLEDPKIKEIAAKHKKTTAQVLIRFHIQRNVTVIPKSMTPAHIVE  300

AKR1B10    273  NIQVFDFKLSDEEMATILSFNRNWRACNVLQSSHLEDYPFNAEY  316
AKR1B15.1  273  NIQVFDFKLSDEEMATILSFNRNWRAFDFKEFSHLEDFPFDAEY  316
AKR1B15.2  301  NIQVFDFKLSDEEMATILSFNRNWRAFDFKEFSHLEDFPFDAEY  344
```

Figure 2:

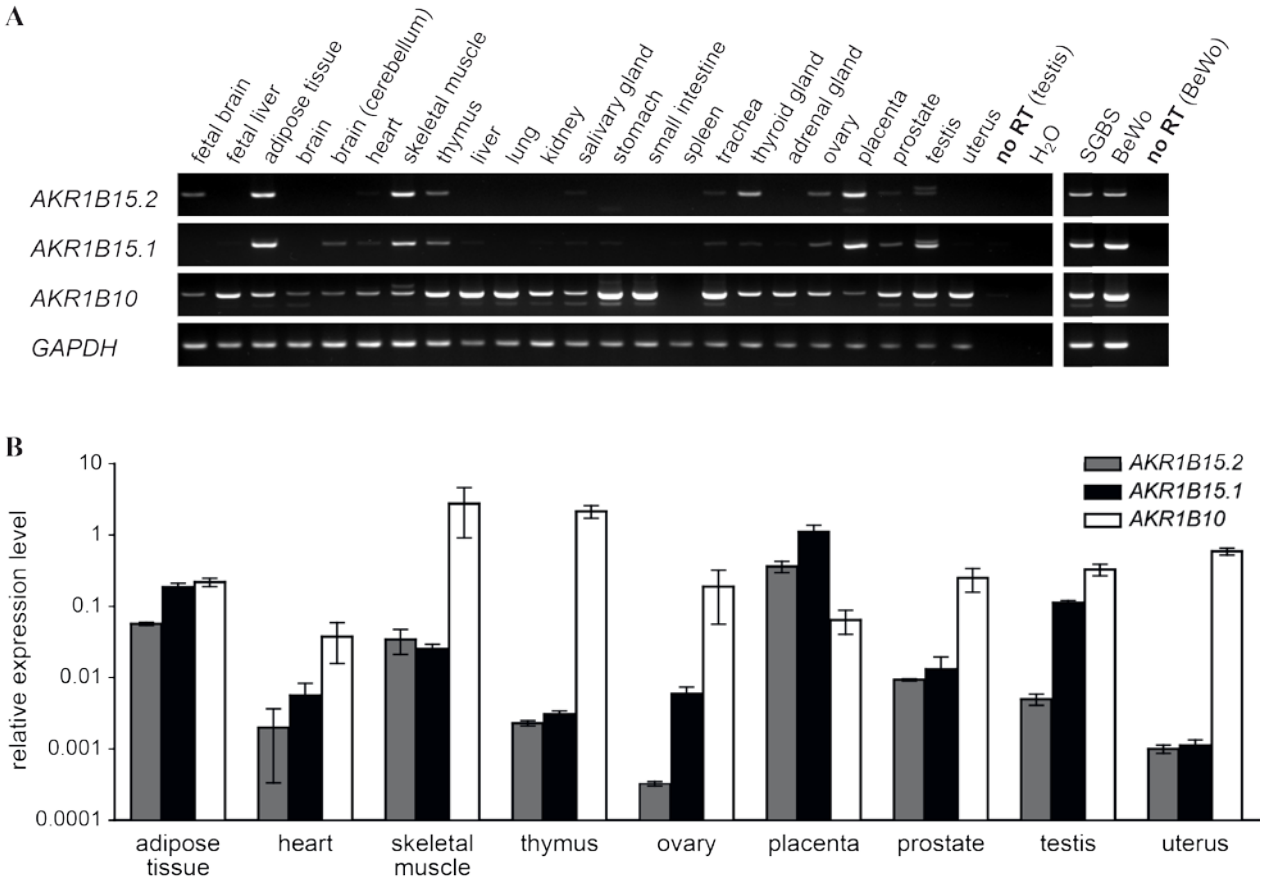
A
fetal brain
fetal liver
adipose tissue
brain
brain (cerebellum)
heart
skeletal muscle
thymus
liver
lung
kidney
salivary gland
stomach
small intestine
spleen
trachea
thyroid gland
adrenal gland
ovary
placenta
prostate
testis
uterus
no RT (testis)
H2O
SGBS
BeWo
no RT (BeWo)
AKR1B15.2
AKR1B15.1
AKR1B10
GAPDH
B
relative expression level
10
1
0.1
0.01
0.001
0.0001
AKR1B15.2
AKR1B15.1
AKR1B10
adipose tissue
heart
skeletal muscle
thymus
ovary
placenta
prostate
testis
uterus

Figure 3:

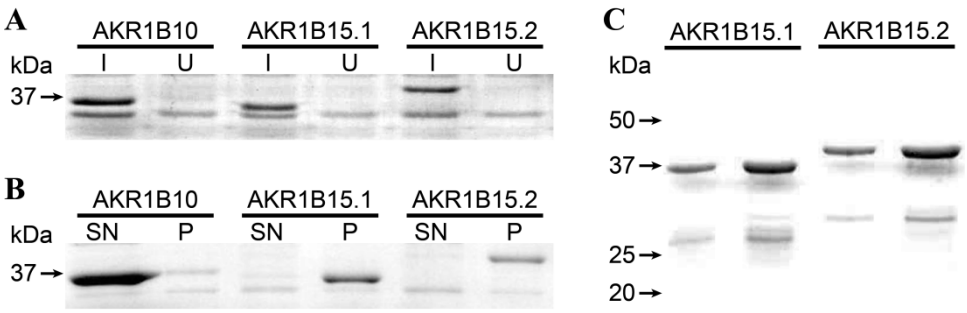
A
AKR1B10
AKR1B15.1
AKR1B15.2
kDa
I
U
I
U
I
U
37
B
AKR1B10
AKR1B15.1
AKR1B15.2
kDa
SN
P
SN
P
SN
P
37
C
AKR1B15.1
AKR1B15.2
kDa
50
37
25
20

Figure 4:

A

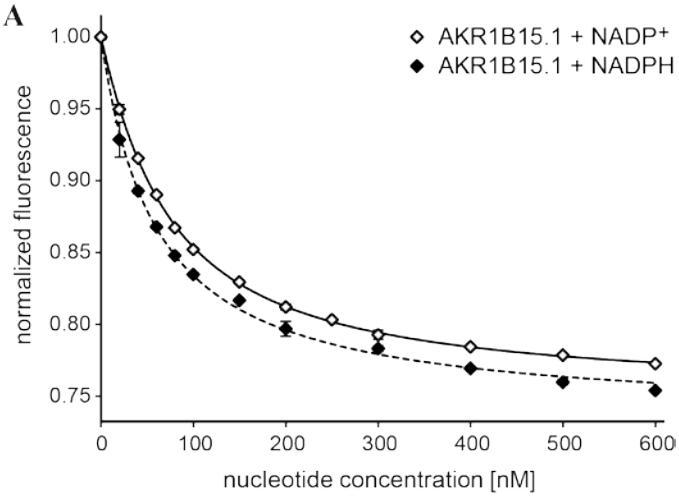

B

	K_d [nM]	max. quenching [%]
NADPH	59 ± 2	26
$NADP^+$	60 ± 4	25
NADH	no binding	< 3
NAD^+	no binding	< 3

Figure 5:

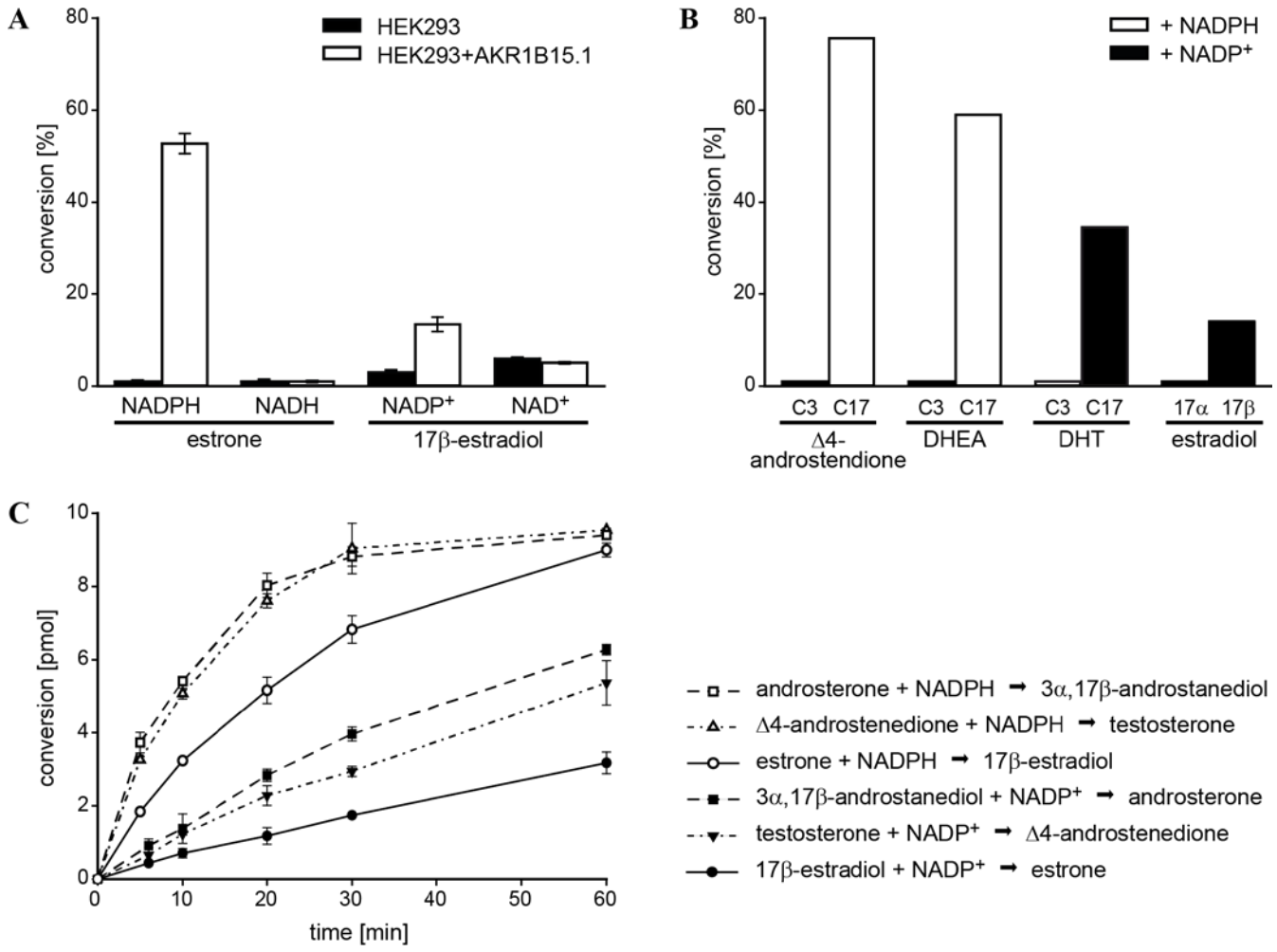
A
HEK293
HEK293+AKR1B15.1
conversion [%]
NADPH
NADH
NADP+
NAD+
estrone
17β-estradiol
B
+ NADPH
+ NADP+
conversion [%]
C3 C17
Δ4-androstendione
DHEA
DHT
17α 17β
estradiol
C
conversion [pmol]
time [min]
androsterone + NADPH → 3α,17β-androstanediol
Δ4-androstenedione + NADPH → testosterone
estrone + NADPH → 17β-estradiol
3α,17β-androstanediol + NADP+ → androsterone
testosterone + NADP+ → Δ4-androstenedione
17β-estradiol + NADP+ → estrone

Figure 6:

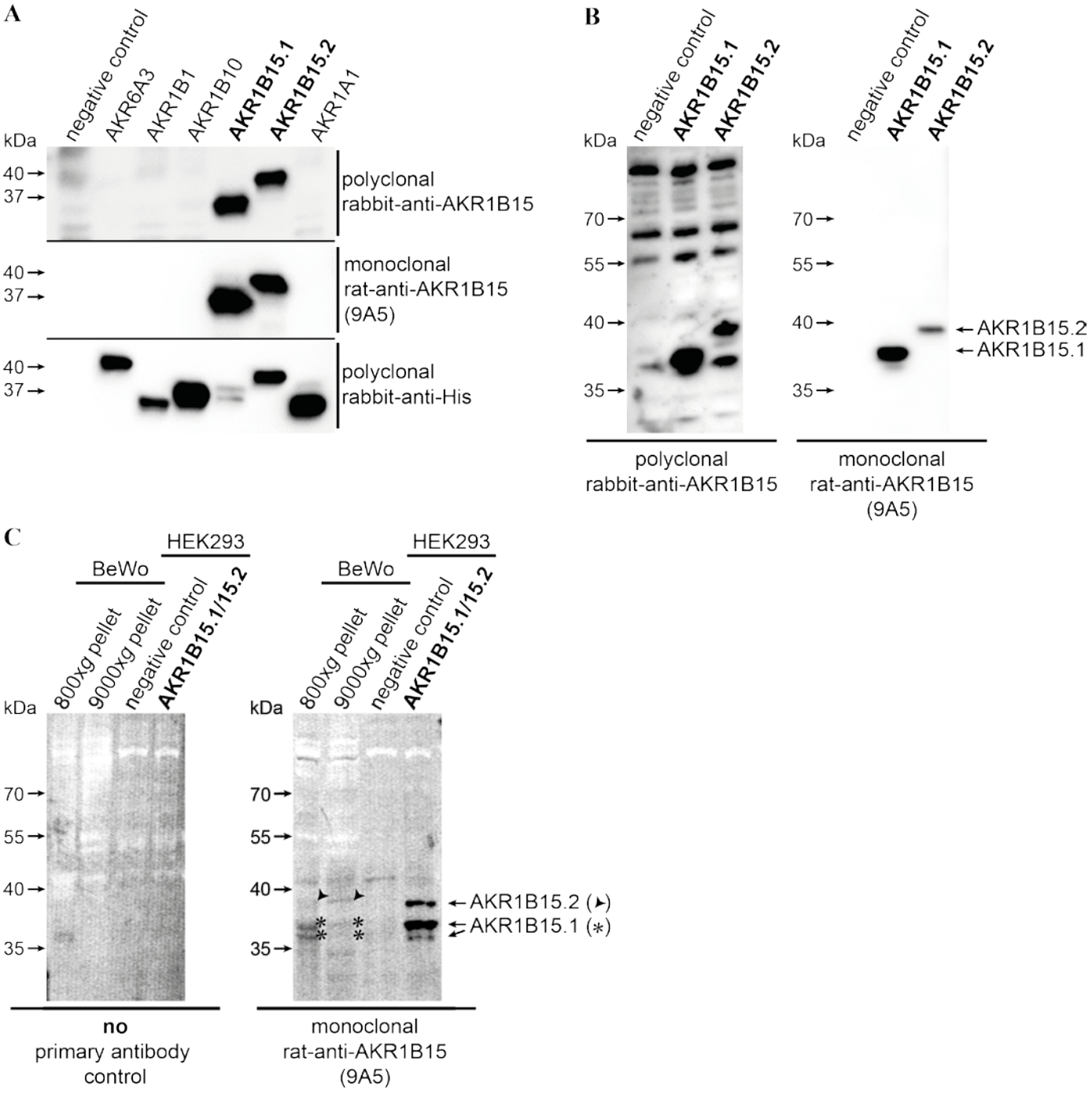
A
negative control
AKR6A3
AKR1B1
AKR1B10
AKR1B15.1
AKR1B15.2
AKR1A1
kDa
40
37
polyclonal
rabbit-anti-AKR1B15
monoclonal
rat-anti-AKR1B15
(9A5)
polyclonal
rabbit-anti-His
B
negative control
AKR1B15.1
AKR1B15.2
kDa
70
55
40
35
polyclonal
rabbit-anti-AKR1B15
monoclonal
rat-anti-AKR1B15
(9A5)
AKR1B15.2
AKR1B15.1
C
HEK293
BeWo
800xg pellet
9000xg pellet
negative control
AKR1B15.1/15.2
kDa
70
55
40
35
AKR1B15.2 (➤)
AKR1B15.1 (*)
no
primary antibody
control
monoclonal
rat-anti-AKR1B15
(9A5)

Figure 7:

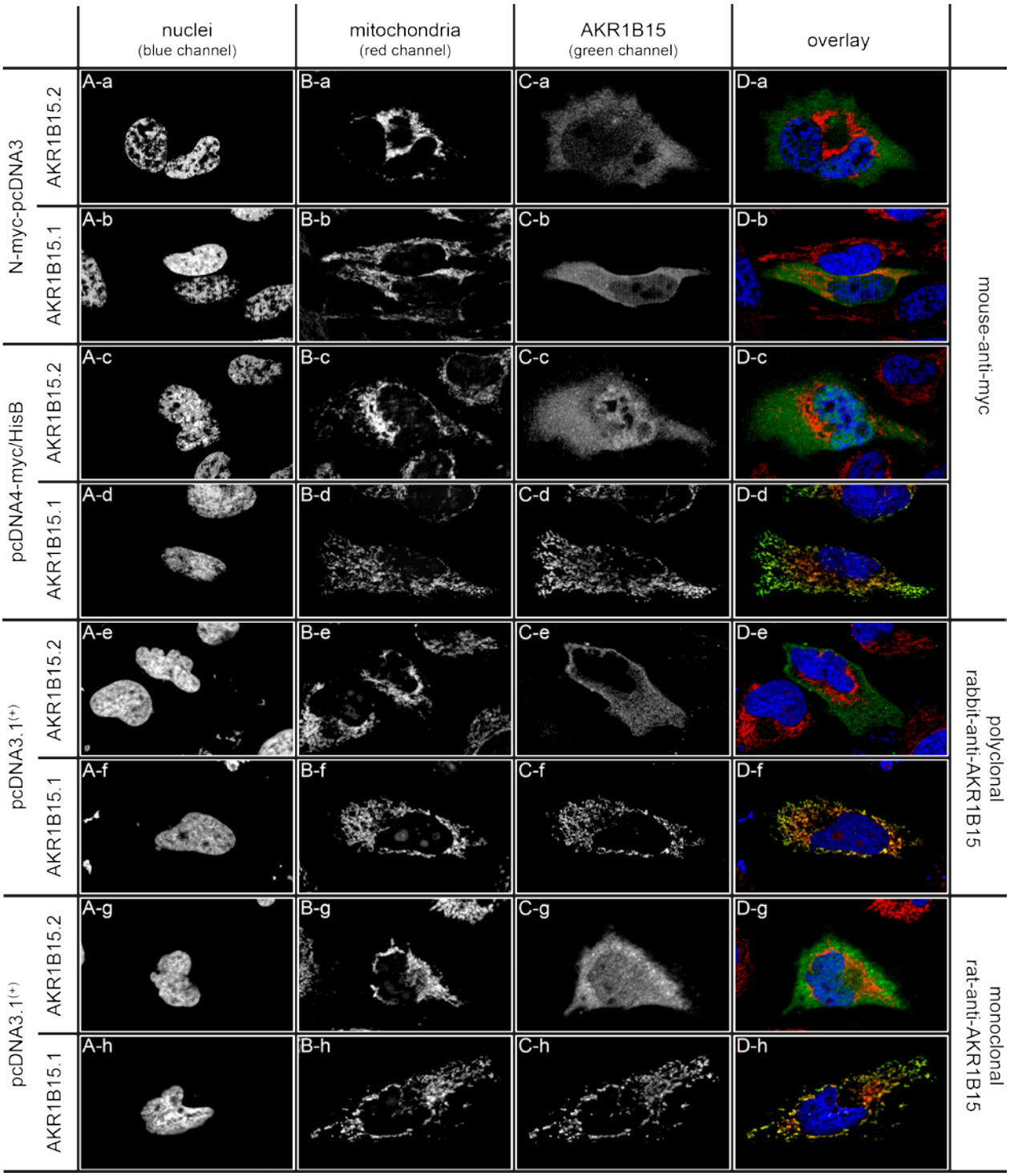
nuclei
(blue channel)
mitochondria
(red channel)
AKR1B15
(green channel)
overlay
N-myc-pcDNA3
pcDNA4-myc/HisB
pcDNA3.1(+)
AKR1B15.2
AKR1B15.1
A-a
B-a
C-a
D-a
A-b
B-b
C-b
D-b
A-c
B-c
C-c
D-c
A-d
B-d
C-d
D-d
A-e
B-e
C-e
D-e
A-f
B-f
C-f
D-f
A-g
B-g
C-g
D-g
A-h
B-h
C-h
D-h
mouse-anti-myc
polyclonal
rabbit-anti-AKR1B15
monoclonal
rat-anti-AKR1B15